AD-A085 477 NAVAL RESEARCH LAB WASHINGTON DC F/G 20/9

DETAILED ATOMIC NEON LTE EMISSION MODEL AND STARK PROFILES FOR --ETC(U)

APR 80 P C KEPPLE, J E ROGERSON

UNCLASSIFIED NRL-MR-4216 SBIE-AD-E000 432 NL

1 OF 1

AD-

A085477

END

DATE

FILMED

7-80

DTIC

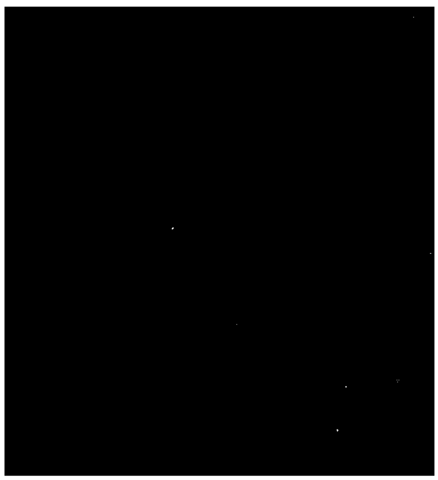

SECURITY CLASSIFICATION OF THIS PAGE (When Data Entered)

REPORT DOCUMENTATION PAGE

READ INSTRUCTIONS BEFORE COMPLETING FORM

1. REPORT NUMBER NRL Memorandum Report 4216	2. GOVT ACCESSION NO. AD-A085 477
3. RECIPIENT'S CATALOG NUMBER	
4. TITLE (and Subtitle) DETAILED ATOMIC NEON LTE EMISSION MODEL AND STARK PROFILES FOR H-LIKE AND He-LIKE NEON AND ARGON	5. TYPE OF REPORT & PERIOD COVERED Final report on an NRL problem.
	6. PERFORMING ORG. REPORT NUMBER
7. AUTHOR(s) Paul C. Kepple and J.E. Rogerson	8. CONTRACT OR GRANT NUMBER(s)
9. PERFORMING ORGANIZATION NAME AND ADDRESS Naval Research Laboratory Washington, D.C. 20375	10. PROGRAM ELEMENT, PROJECT, TASK AREA & WORK UNIT NUMBERS NRL Problem 67-0858-0-0
11. CONTROLLING OFFICE NAME AND ADDRESS	12. REPORT DATE April 25, 1980
	13. NUMBER OF PAGES 64
14. MONITORING AGENCY NAME & ADDRESS(if different from Controlling Office)	15. SECURITY CLASS. (of this report) UNCLASSIFIED
	15a. DECLASSIFICATION/DOWNGRADING SCHEDULE

16. DISTRIBUTION STATEMENT (of this Report)

Approved for public release; distribution unlimited.

17. DISTRIBUTION STATEMENT (of the abstract entered in Block 20, if different from Report)

18. SUPPLEMENTARY NOTES

Work funded by the Los Alamos Scientific Laboratory.

19. KEY WORDS (Continue on reverse side if necessary and identify by block number)

Dense plasmas
Stark broadening
Radiation

20. ABSTRACT (Continue on reverse side if necessary and identify by block number)

A neon LTE model based on actual atomic data and including a large number of excited levels and lines, especially in the He-like and H-like stages, is described. Results are given for line and continuum emissions vs. frequency. Stark broadened line profiles for H-like and He-like neon and argon atoms are presented as functions of frequency, electron temperature, and electron density.

CONTENTS

AN ASSESSMENT OF PHYSICS RESEARCH OPPORTUNITIES AVAILABLE FROM RAPID HEATING AND COOLING

INTRODUCTION

The radiation emitted from laser-produced plasmas is the major diagnostic tool for obtaining information on the properties of the compressed emitting region. From suitably chosen line ratios, line-to-continuum measurements, and line profiles, plasma parameters such as electron density and temperature can be inferred. For example, the ratio of the H-like $2p(^2P) \rightarrow 1s(^2S)$ emission to the He-like $1s2p(^1P) \rightarrow 1s^2(^1S)$ emission gives an estimate of electron temperature[1]. A detailed study of line intensities and profiles represents, at present, the only comprehensive method of obtaining compression information. Fitting of theoretical Stark-broadened profiles to experimental profiles gives a measure of electron density[2]. A study of x-ray line profiles, Stark broadening, and opacity broadening give direct measurements of the compressed density ρ and the product ρR, where R is the radius of the compressed plasma core. The product ρR is a parameter of significant importance in inertially confined fusion; e.g., it is a critical quantity in determining the neutron yield in a compressed DT plasma[3]. A study of x-ray continuum edge shifts due to pressure ionization also yields a measure of the compressed core plasma density[4]. Hence, it is readily apparent that analyses of the emissions from laser-heated plasmas provide the definitive measurements of the significant parameters of the plasmas. It is therefore extremely important, because of the transient and irreproducible nature of laser driven plasma implosion experiments, to collect as large an amount of reliable spectral data as possible on each experiment, and to apply a wide variety of diagnostic techniques to analyze these data and gain a comprehensive understanding for characterizing the laser driven plasma fusion process.

Manuscript submitted February 29, 1980.

In the present experimental environment, He-like profiles are crucial to the analyses. For example, in the current series of Argon experiments, it has not been possible to achieve hot enough electron temperatures to produce predominantly H-like Argon atoms, and hence H-like spectra. H-like lines are optically thick and distorted by overlapping lines or contaminent emission, or are too weak. He-like lines, on the other hand, are readily identified and analyzed. In the past, conditions of temperature, density, and the technology of providing certain emitting species have limited the range of diagnostic techniques. However, the analysis of He-like spectra has provided an extended diagnostic range. With the same concepts of analysis extended to lines from other ionization stages, a more self consistent picture of the emitting plasma can be drawn.

In the theoretical work, radiation as a diagnostic tool has not been adequately treated. For example, an LTE model based on a complete level structure using real data (and thus generating realistic partition functions, for example) has never been applied to the problem of laser plasma simulation. That is one of the problems this report attempts to address. A Neon LTE package is presented which is based on actual atomic data and includes a large number of levels and lines, especially in the He-like and H-like stages. These data are then used to compute total line emissions and emission coefficients for line, free-bound and free-free processes as functions of frequency. A similar package for Argon is to be generated in the near future.

The LTE assumption is clearly not valid for a complete treatment of the laser emission problem. For example, under present experimental

conditions involving Argon plasmas, the compressed density was less than that required to establish LTE in at least the first three levels of H-like Argon. Skupsky[5] has shown that the 2p level of H-like Neon must be treated as having a non-LTE relation to the H-like ground state in many Neon plasma emission experiments.

Brief mention is made in this report of a non LTE radiation transport code that will be implemented at a later data. This program uses a collisional-radiative model (CR) of the Neon atom, and, like the LTE package mentioned earlier, is based on real atomic data (energy levels, collisional excitation rates, etc.) and has a complex level structure. Selected diagnostic lines are transported utilizing a ray tracing algorithm in a cylindrical geometry. Stark and collisional broadening, as well as self-absorption, are included. The effects of optical thickness and radiation transport on the emitted spectra are studied.

References

1. J. Davis, K. G. Whitney, and J. P. Apruzese, JQSRT 20, 353 (1978).
2. K. B. Mitchell, D. B vanHusteyn, G. H. McCall, P. Lee, and H. R. Griem, Phys. Rev. Lett. 42, 232 (1974); B. Yaakobi, D. Steel, E. Thorsos, A. Hauer, and B. Perry, Phys. Rev. Lett. 39, 1526 (1977).
3. G. S. Fraley, E. J. Linnebur, R. J. Mason, and R. L. Morse, Phys. Fluids 17, 474 (1974).
4. C. M. Lee and A. Hauer, Appl. Phys. Lett. 33 (8), 692 (1978).
5. S. Skupsky, Optically Thick Spectral Lines as a Diagnostic Tool for Laser Imploded Plasmas, Report No. 80, Laboratory for Laser Energetics, University of Rochester, May 1978.

II. NEON LTE EMISSION MODEL

In order to characterize the emissions of hot plasmas, a model has been developed to calculate the emission coefficient (emission/volume sec hz steradian) of a plasma assumed to be in LTE for various values of electron density and temperature. For a given representation of an atom, the program computes partition functions for each ionization stage, which are then used to solve the Saha-Boltzmann equations and obtain ground-state and excited-level population densities for the various ionization stages. These population densities are then used to calculate emission coefficients $j(\nu)$ for free-free, free-bound, and bound-bound emission processes.

The partition functions U are given by

$$U\,(i) = \sum_{j=o}^{n} g_{ij} \exp\,(-E_{ij}/kT) + U^1(i) \tag{1}$$

where g_{ij} and E_{ij} are the statistical weights and excitation energies of ionization stage i, and kT is the electron temperature. $U^1(i)$ is a term introduced by Griem (Plasma Spectroscopy, McGraw-Hill Book Company, New York, 1964) to take into account those levels omitted in the sum in the first term;

$$U^1(i) = \frac{2}{3}\,(2S_1 + 1)\;(2L_1 + 1)\left[\frac{Z^2 E_H}{\Delta E(i)}\right]^{3/2} \exp\left(-\frac{I_p^1(i)}{kT}\right), \tag{2}$$

where S_1 and L_1 are the spin and angular momentum of the ground state of the next higher ionization stage i + 1, E_H = 13.6 eV, and the reduction in the ionization potential $I_p(i)$ is given by

$$\Delta E(i) = \text{minimum} \left\{ \frac{Ze^2}{D}, \frac{3}{2} \frac{Ze^2}{\rho_o} \right\} \quad (3)$$

as recommended by Stewart and Pyatt (Lowering of Ionization Potentials in Plasmas, JILA Report No. 54, University of Colorado, Boulder, Colorado, November 29, 1965). Here D is the Debye length, and ρ_o is the ion sphere radius $(3/4 \pi N_e)^{1/3}$ for electron density N_e. $I_p^1(i)$ is the reduced ionization potential given by

$$I_p^1(i) = I_p(i) - \Delta E(i). \quad (4)$$

The ratio of the total population densities of adjacent ionization stages is given by the Saha equation

$$\frac{N(i+i)}{N(i)} = \frac{2(2\pi m\ k\ T)^{3/2}}{N_e\ h^3} \frac{U(i+i)}{U(i)} \exp\left(-\frac{I_p^1(i)}{kT}\right), \quad (5)$$

where N(j) is the density of ionization stage j, m is the electron mass, and h is Planck's constant. Once the N(j) are determined, the ground state and excited level population densities are calculated from the Boltzmann relations.

The total line emission from a given transition is given by

$$E_{nm} = \frac{N_n}{4\pi} A_{nm}\, h\nu_{nm} \ (\text{energy/cm}^3 \text{ sec ster.}), \quad (6)$$

where N_n is the excited level population density, A_{nm} is the Einstein A coefficient for spontaneous emission from level n to level m, and $h\nu_{nm}$ is the energy of the transition. This quantity is computed for every line included in the atomic model, and the results are summed to obtain the total line emissions.

In LTE, the emission coefficient for a given process can be calculated from

$$j(\nu) = k(\nu)\; B_o\;(\nu, T)\;\left[1 - \exp\;(-h\nu/kT)\right], \tag{7}$$

where $k(\nu)$ is the absorption coefficient for the same process, and B_o (ν, T) is the Planck distribution function. Using this relation and the usual expressions for the absorption coefficients for the various processes (e.g., W. J. Karzas and R. Latter, Astrophys. J. Supplement 55, Vol. VI, p. 167-212, May, 1961), emission coefficients can be defined for the various processes.

For bound-bound (line) emission processes,

$$j^{bb}(\nu) = \frac{N_n}{4\pi}\; A_{nm}\; h\,\nu_{nm}\; \phi\;(\nu), \tag{8}$$

where $\phi\;(\nu)$ is the line profile function, defined such that

$$\int \phi\;(\nu)\; d\nu = 1.$$

For free-bound processes,

$$j^{fb}\;(\nu) = \frac{2\,\nu^3}{c^2}\; e^{-h\nu/kT} \sum_{i,j} N_{ij}\; \sigma^K(n\ell \rightarrow E)\; G_{bf}\;(n,\; \ell,\; \nu), \tag{9}$$

where N_{ij} is the density of excitation level j in ion stage i (j = o is the ground state), σ^K $(n\ell \rightarrow E)$ is the Kramers semi-classical bound-free cross section (as given by Karzas and Latter), and G_{bf} (n, ℓ, ν) is the bound-free Gaunt factor (also taken from Karzas and Latter).

For free-free emission,

$$j^{ff}(\nu) = \frac{16\;\pi\;\; e^6}{3\sqrt{3}\;\; mc^3} \left(\frac{1}{2\pi\;\; mkT}\right)^{\frac{1}{2}} N_e\; N_i\; Z^2\; e^{-h\nu/kT}\; G_{ff}(\nu,\; T,\; Z), \tag{10}$$

where N_i is the density of ions of charge Z, and $G_{ff}(\nu, T, z)$ is the free-free Gaunt factor (from Karzas and Latter). As $\nu \to o$, this last expression becomes a constant. This is non-physical, since, for frequencies below the plasma frequency ν_p, the plasma becomes optically thick and the emission is very small. Hence, for frequencies $\leq \nu_p$, $j^{ff}(\nu)$ is set equal to zero. For frequencies small, but still larger than ν_p, the free-free emission is calculated from

$$j^{ff}(\nu) = \frac{\nu_p^2}{2\pi c^3} \frac{kT}{T_c} \left(1 - \frac{\nu_p^2}{\nu^2}\right)^{\frac{1}{2}}, \tag{11}$$

$$\text{where } T_c = \frac{4\pi\sqrt{3}\, Ze^2}{9\sqrt{\pi}\, m} \left(\frac{m}{2kT}\right)^{3/2} \omega_p^2 \; G_{ff}(\nu, T, z) \tag{12}$$

is the reciprocal of the effective electron-ion collision frequency. (G. Bekefi, Radiation Processes in Plasmas, John Wiley and Sons, New York, 1966). At some frequency ν_o, the two expressions for $j^{ff}(\nu)$ are equal. For the interval $\nu_p \leq \nu \leq \nu_o$, the low frequency form is used; at higher frequencies, the other form is used.

The Neon atomic model is based on data from M. L. Weise, M. W. Smith. and B. M. Glennon (NSRDS-NBS 4, Atomic Transition Probabilities, Vol. 1, May 20, 1966), except for the K shell, where averaged energy levels (from P. C. Kepple, NRL) are used to extend the level structure up to n = 10. Also, for Neon X, data from R. J. Kelly and L. J. Palumbo (NRL Report 7599, Atomic and Ionic Emission Lines Below 2000 Angstroms; Hydrogen Through Krypton, June 1973) are used. Einstein A values are obtained from Z^4 scaling of hydrogenic values.

Table 1 gives a resume of the line and level structure presently included in the model. In the selection, an attempt was made to include at least the most important lines. The scarcity of lines for Neon VII and VIII is due to the fact that only a small amount of data was given.

Sample results of calculations using this model will now be presented. Figure 1 shows a calculation of the average charge $\bar{Z}$ of the Neon atom vs. kT for several values of electron density N_e. As expected, a higher N_e gives a lower $\bar{Z}$ for a given value of kT for $N_e = 10^{21} - 10^{23}$. The higher $\bar{Z}$ values at lower kT for $N_e = 10^{24}$ are the results of continuum lowering which completely removed the lower ionization stages. Also shown is a coronal calculation of $\bar{Z}$ (V. L. Jacobs, J. Davis, J. E. Rogerson, and M. Blaha, Astrophys. J. 230, 627. (1979).

Table 2 shows a $\bar{Z}$ comparison between this LTE model and a Collisional Radiative Equilibrium (CRE) model (D. Duston, NRL, unpublished). Since the CRE uses the total ion density N_T as a parameter, a direct comparison is difficult; however, fully stripped Neon corresponds to $N_e = 10\ N_T$, so the calculations were grouped in this manner. Generally, the results are equal at 100 eV; the CRE result is then lower and approaches the LTE $\bar{Z}$ as kT increases. All other parameters being equal, LTE usually produces a higher population of excited levels in a given ionization stage than CRE. Since these excited levels are more easily ionized, a higher $\bar{Z}$ results in LTE. As N_T or kT increases, the two models should approach each other; this is especially seen at the highest densities except at 100 eV. It should be noted that the level structure in the two Neon models is not the same, and the CRE model did not include continuum lowering.

Figure 2 shows a plot of $j^{fb}(\nu)$ at kT = 100 eV for $N_e = 10^{21}$ cm^{-3} and 10^{23} cm^{-3}. The slight shift toward lower $h\nu$ of the higher density curve is due to continuum lowering causing the edges to shift to lower energies. The differences in the results for low frequencies arises from the fact that $\overline{Z} = 8$ for $N_e = 10^{21}$ and $\overline{Z} = 7.4$ for $N_e = 10^{23}$. Hence the lower density curve reflects the Neon IX level structure much more than the higher density curve which is influenced by the Neon VIII structure, where few levels are included.

Figure 3 shows $j^{fb}(\nu)$ at $N_e = 10^{23}$ cm^{-3} at kT = 10, 100, and 1000 eV. These results indicate the presence of higher ionization stages as kT increases; at 10 eV there is no K edge, while at 100 eV and 1000 eV the K edge emission is prominent. Hence, as kT increases, the curves shift to higher frequency.

Figure 4 shows a calculation of the ratio of the 2p - 1s resonance emission in the hydrogen-like and helium-like stages of Neon vs. kT for different N_e values. Since the ratio of the population densities of adjacent ionization stages varies as $1/N_e$ in the Saha equation, a strong density dependence of this ratio is expected. This is indeed reflected in these results. There is also a very strong temperature dependence. Also shown is a coronal calculation of this ratio, which is density independent. Since LTE produces a much higher excited-level-population density than a coronal calculation, it might be expected that the emission ratio would also be higher for LTE.

Figure 5 shows the 3p - 1s emission ratio for the same two ionization stages. A coronal calculation is also included, and a similar calculation by Yaakobi, et.al. (B. Yaakobi, D. Steel, E. Thorsos, A. Hauer, B. Perry,

S. Skupsky, J. Geiger, C. M. Lee, S. Letzring, J. Rizzo, T. Mukaiyama, E. Lazarus, G. Halpern, H. Deckman, J. Delettrez, J. Soures, and R. McCrory, Phys. Rev. A. 19, 1247, (1979)), is shown for comparison sake. They seem to use a combination of the Saha and corona models to derive this result, which is apparently independent of density.

Figure 6 shows a plot of the normalized total line emission vs. kT for several values of N_e; this plot represents the sum over the emissions of the 192 lines in the model divided by the product $N_e N_T$, where N_T is the total ion density. In all these plots, K shell emission does not dominate for kT less than 100 eV, but for kT greater than 100 eV, the emission is almost totally from Neon IX and X. The transition from L shell to K shell emission dominance is most noticeable at $N_e = 10^{21}$ cm^{-3} and 10^{22} cm^{-3}.

Calculations of line emission spectra from Eq. (8) have been made using two types of line shape functions $\phi(\nu)$. The first profile assumes Stark broadening, and the Stark width computations are based largely on the work of H. R. Griem, M. Blaha, and P. C. Kepple (Phys. Rev. A 19, 2421 (1979)). The electronic Holtsmark field is taken to be

$$F_o = 2.603 \, e \, N_e^{2/3} \tag{13}$$

while the ion field is given by

$$F_z = Z^{1/3} F_o. \tag{14}$$

A hydrogenic Stark shift is then given by

$$\Delta \omega_s = \frac{3e \, a_o F}{\hbar Z} \, n \, (n-1), \tag{15}$$

where e is the electronic charge, a_o is the Bohr radius, F is the sum of F_z and F_o, and n is the principal quantum number of the excited level.

The Stark profile function is

$$\phi_s\ (\omega^1) = \frac{3}{4|\omega^1|} \left|\frac{\Gamma_s}{\omega^1}\right|^{3/2} \exp\left(- \left|\frac{\Gamma_s}{\omega^1}\right|^{3/2}\right) , \tag{16}$$

where $\omega^1 = \hbar\ (\omega - \omega_o)$, ω_o is the line center frequency, and Γ_s is the Stark shift of the line (B. F. Rosznyai, JQSRT <u>19</u>, 641, 1978).

The second profile used in these calculations is the Voigt profile, where

$$\phi(\nu) = U(a,x) \tag{17}$$

is the Voigt function. The parameters a and x are defined by

$$a = (\Delta\ \nu_R + \Delta \nu_C) \ /\ \Delta\ \nu_D \tag{18}$$

$$x = (\nu - \nu_o)\ /\ \Delta\ \nu_D$$

Here $\Delta\ \nu_R$ is the natural line width, $\Delta\ \nu_C$ is the collisional line width, and $\Delta\ \nu_D$ is the Doppler width. Because of the added complication of computing $\Delta\ \nu_C$ in LTE, the parameter was arbitrarily set to 0.5 for these calculations. The Voigt function U(a,x) was evaluated by use of an algorithm taken from A. K. Hui, B. H. Armstrong, and A. A. Wray, JQSRT <u>19</u>, 509 (1978).

Figure 7 shows a comparison of spectra from the two profiles for Neon at an electron density of 10^{23} cm^{-3} and kT = 1 keV. At each frequency, Eq. (8) is evaluated for each line in the atomic model, and the results are summed to give a total $j^{bb}(\nu)$. However, for this temperature and density, the emission comes almost entirely from the hydrogen-like Neon IX stage.

Hence, the 2p-1s emission near 1022 eV, and the 3p - 1s emission near 1211 eV can be identified. The lines at lower energy are transitions between excited levels.

Due to the fact that the Stark widths are much broader than Doppler widths, the Stark spectrum is much smoother due to the overlapping of many lines. The Voigt function peaks at line center, whereas, from Eq. (16), the Stark function peaks at $\approx 0.77\ \Gamma_s$ from line center and goes to zero at line center.

The results presented in the preceding paragraphs are typical of the many calculations done at several N_e and kT values and are given as examples of the kind of analyses that can be performed with this program.

It must be emphasized that the quantities calculated with this program are local variables; they are typically emissions per unit volume. Hence, this is effectively a zero-dimensional model. In any real plasmas of these densities and temperatures, opacity and radiation transport effects must be included. This program is thus visualized as a part of a larger program which does incorporate these effects. As of this writing, this code is being used in conjunction with some hydrodynamics codes at the Los Alamos Scientific Laboratory (LASL).

TABLE I

Brief resume of the structure of the Neon Atomic Model

NEON ATOMIC MODEL
(data source: M.L. Weise, M.W. Smith, & B.M. Glennon, NSRDS-NBS 4, ATOMIC TRANSITION PROBABILITIES, vol. 1, May 20,1966)

ION. STAGE	NO. EXCITED LEVELS	NO. LINES
I	9	6
II	18	14
III	18	18
IV	16	13
V	15	13
VI	9	11
VII	5	3
VIII	4	6
IX*	15	54
X*	15	54
	TOTAL	192

* Additional Averaged n-level data (NRL)

TABLE II

Comparison of average charge results from LTE and CRE Models

$\bar{Z}$ COMPARISON

kT(eV) ⟶

	100 eV	300 eV	500 eV	800 eV
CORONAL	8.0	8.5	9.2	9.8
CRE $N_T = 10^{20}$	8.0	8.5	9.2	9.8
LTE $N_e = 10^{21}$	8.0	10.0	10.0	10.0
CRE $N_T = 10^{21}$	7.9	8.7	9.5	9.9
LTE $N_e = 10^{22}$	7.9	9.8	9.9	10.0
CRE $N_T = 10^{22}$	7.6	8.8	9.6	9.9
LTE $N_e = 10^{23}$	7.4	9.6	9.7	9.8
CRE $N_T = 10^{23}$	7.0	8.4	9.3	9.7
LTE $N_e = 10^{24}$	6.2	8.2	9.3	9.6

CRE = COLLISIONAL RADIATIVE EQUILIBRIUM

LTE = LOCAL THERMODYNAMIC EQUILIBRIUM

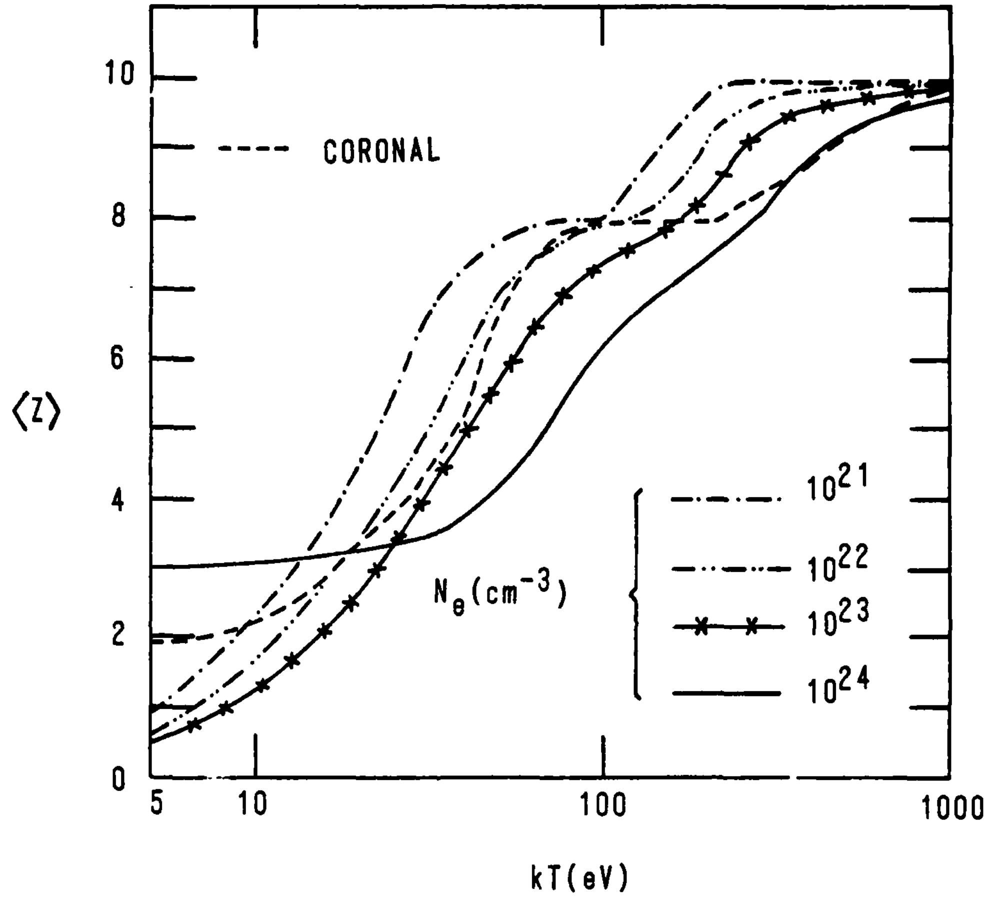

Fig. 1 - Average charge vs. kT for several electronic densities. A coronal result is also shown.

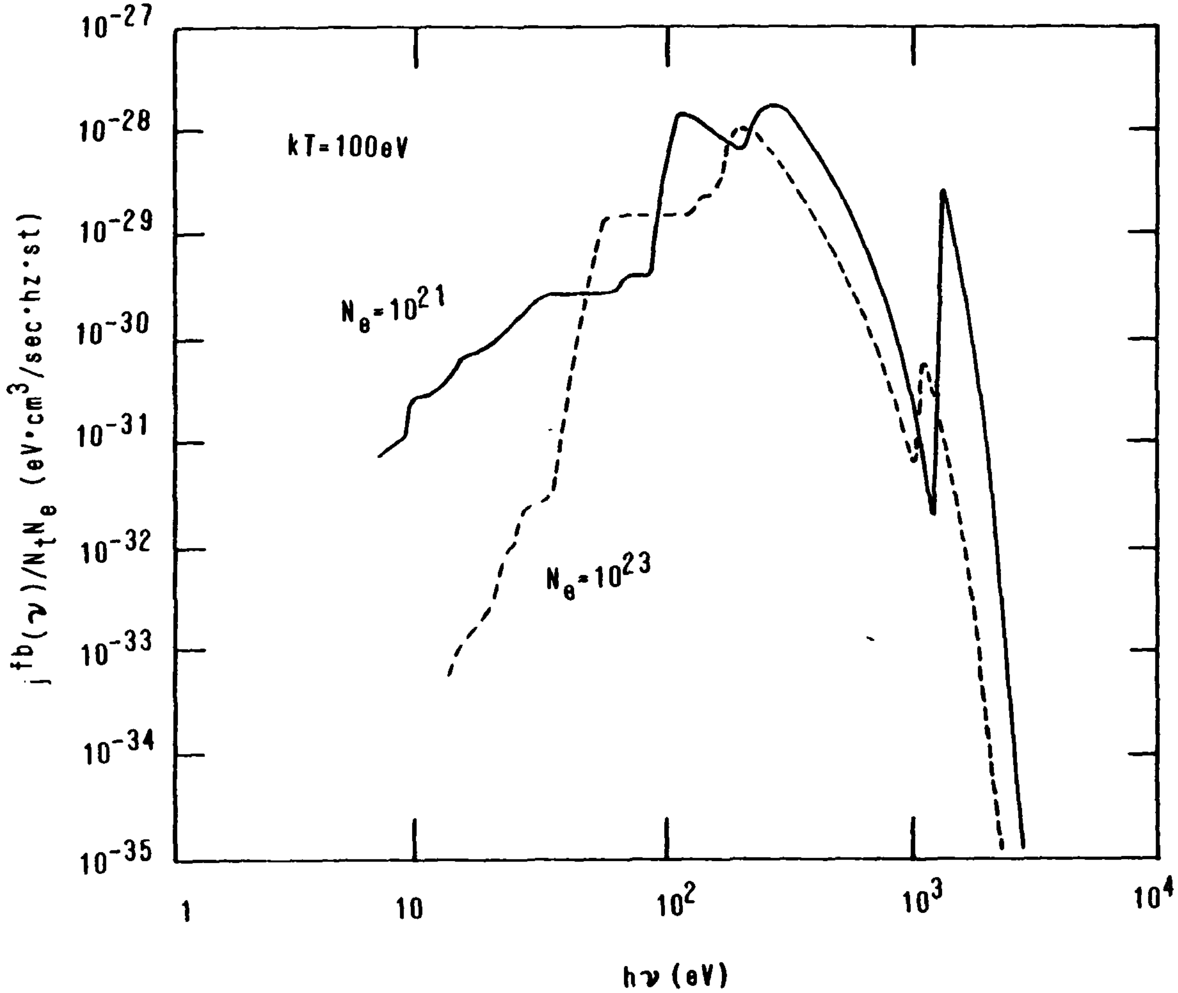

Fig. 2 - Normalized free-bound emission coefficient vs. frequency at kT = 100 eV for $N_e = 10^{21}$ cm^{-3} and 10^{23} cm^{-3}

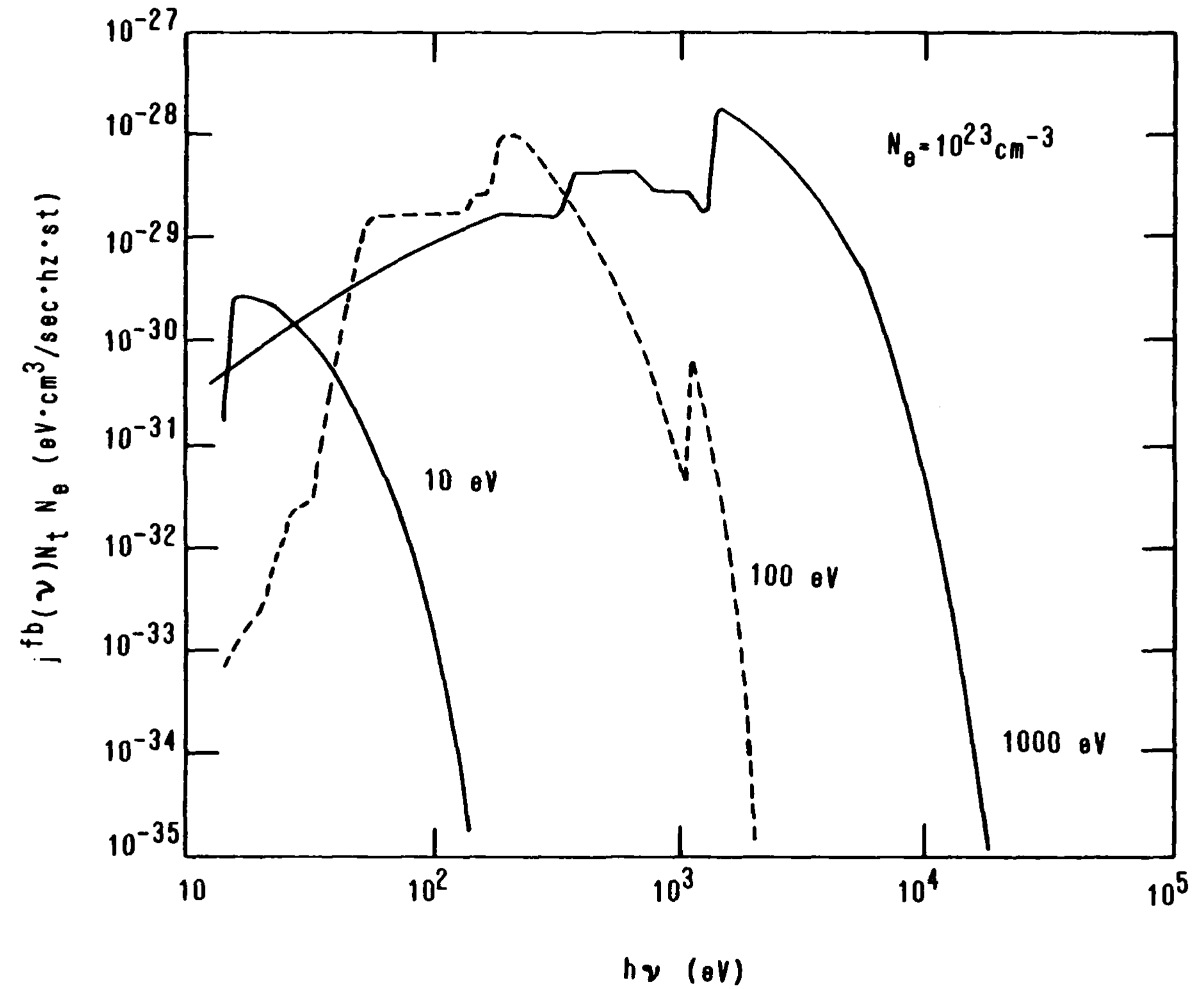

Fig. 3 - Normalized free-bound emission coefficient vs. frequency for $N_e = 10^{23}$ cm^{-3} and kT = 10, 100, and 1,000 eV

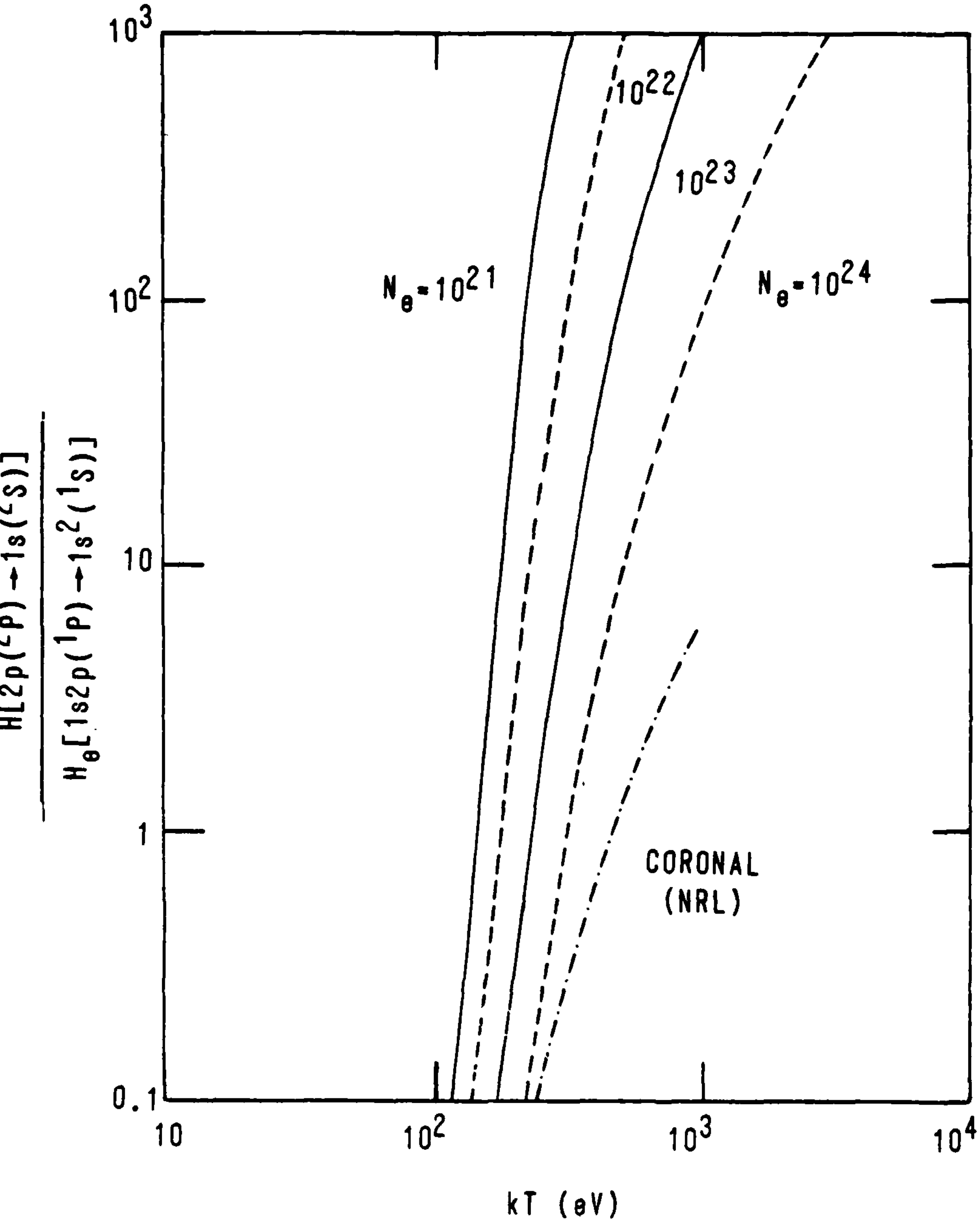

Fig. 4 - Ratio of the H-like and He-like 2p-1s resonance lines vs. kT for several electron densities. A coronal result is also shown.

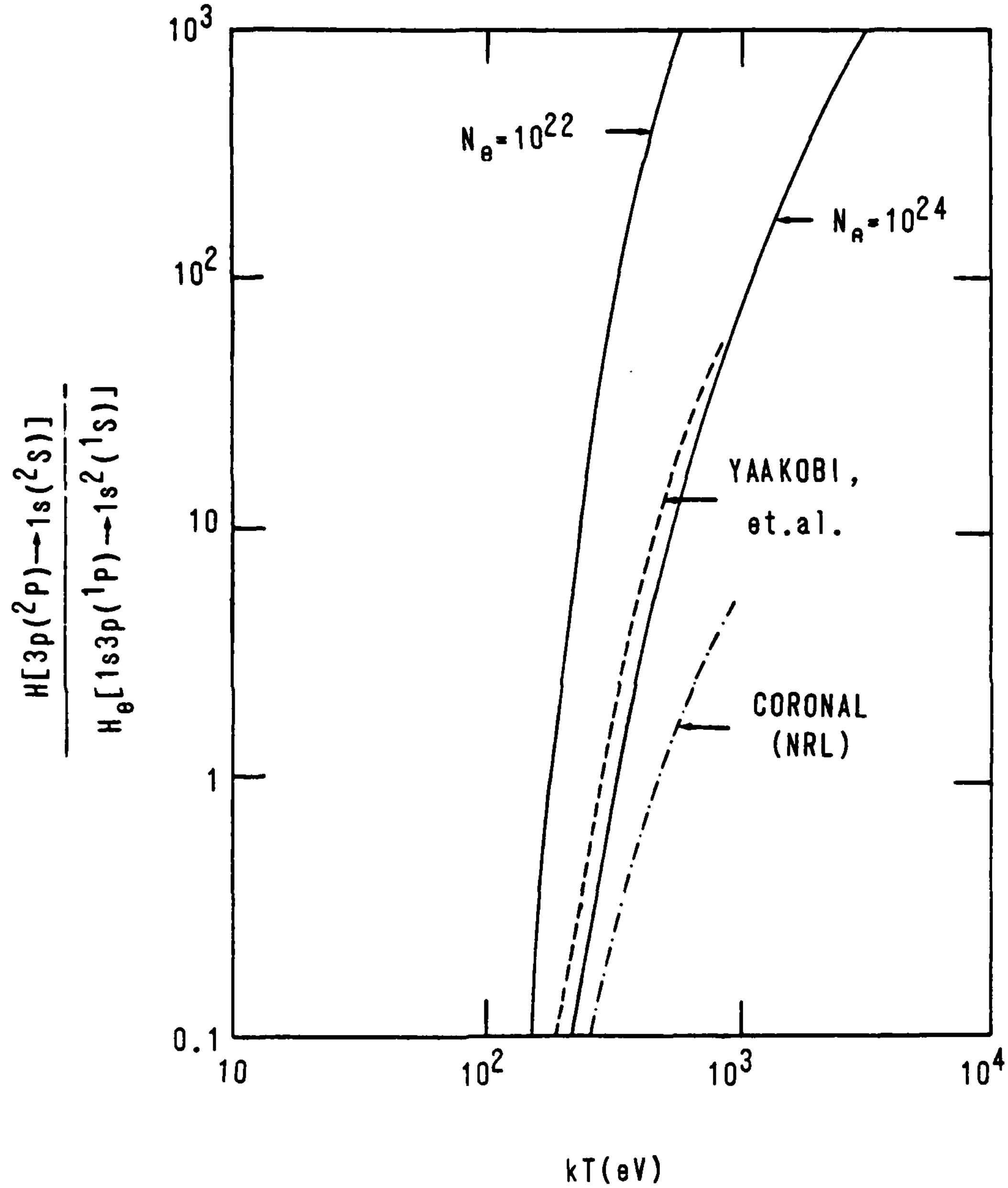

Fig. 5 - Ratio of H-like and He-like 2p-1s lines vs. kT for two electron densities. Also shown is a coronal result and a calculation by Yaakobi, et.al.

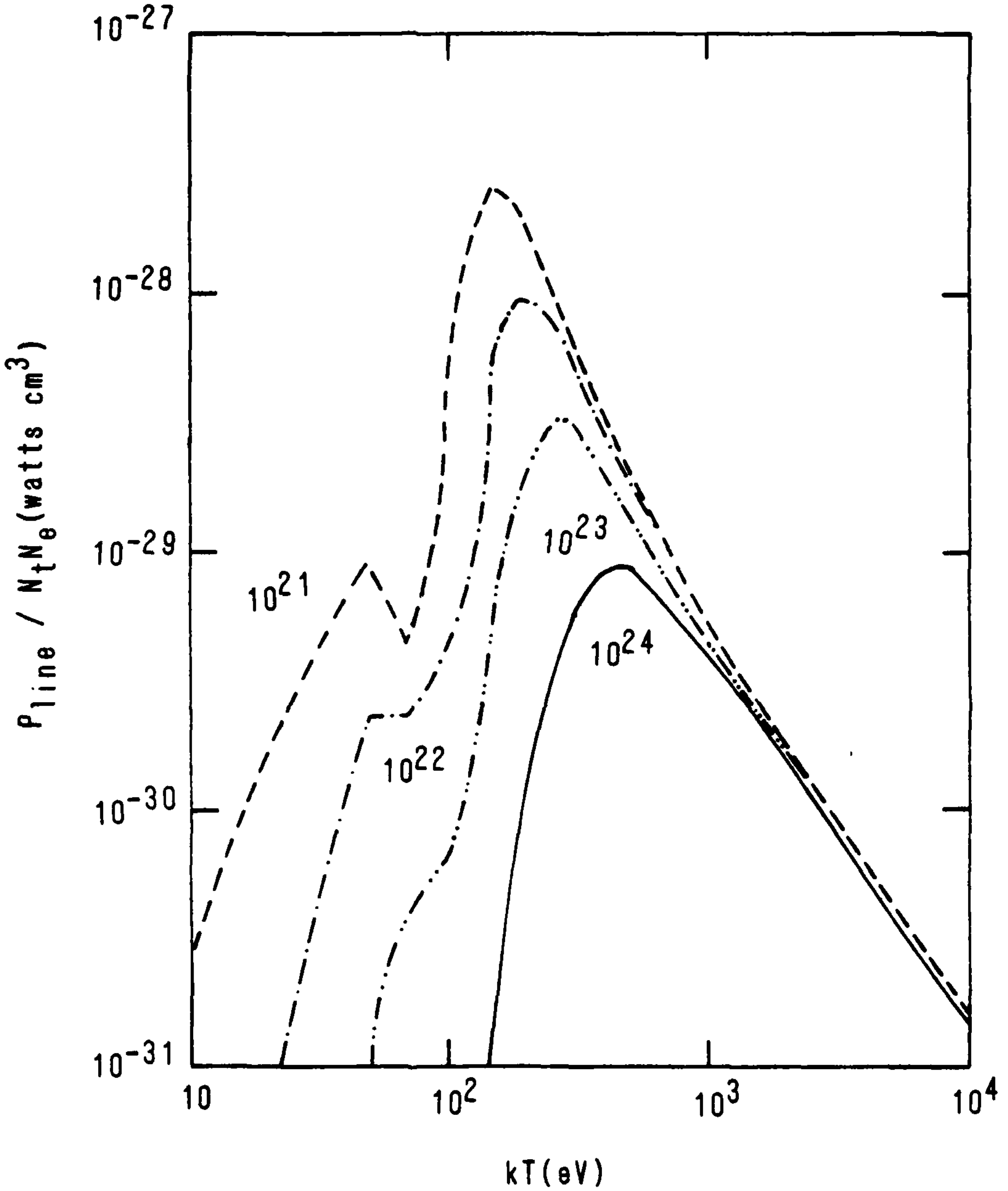

Fig. 6 - Normalized total line emission vs. kT for several electron densities

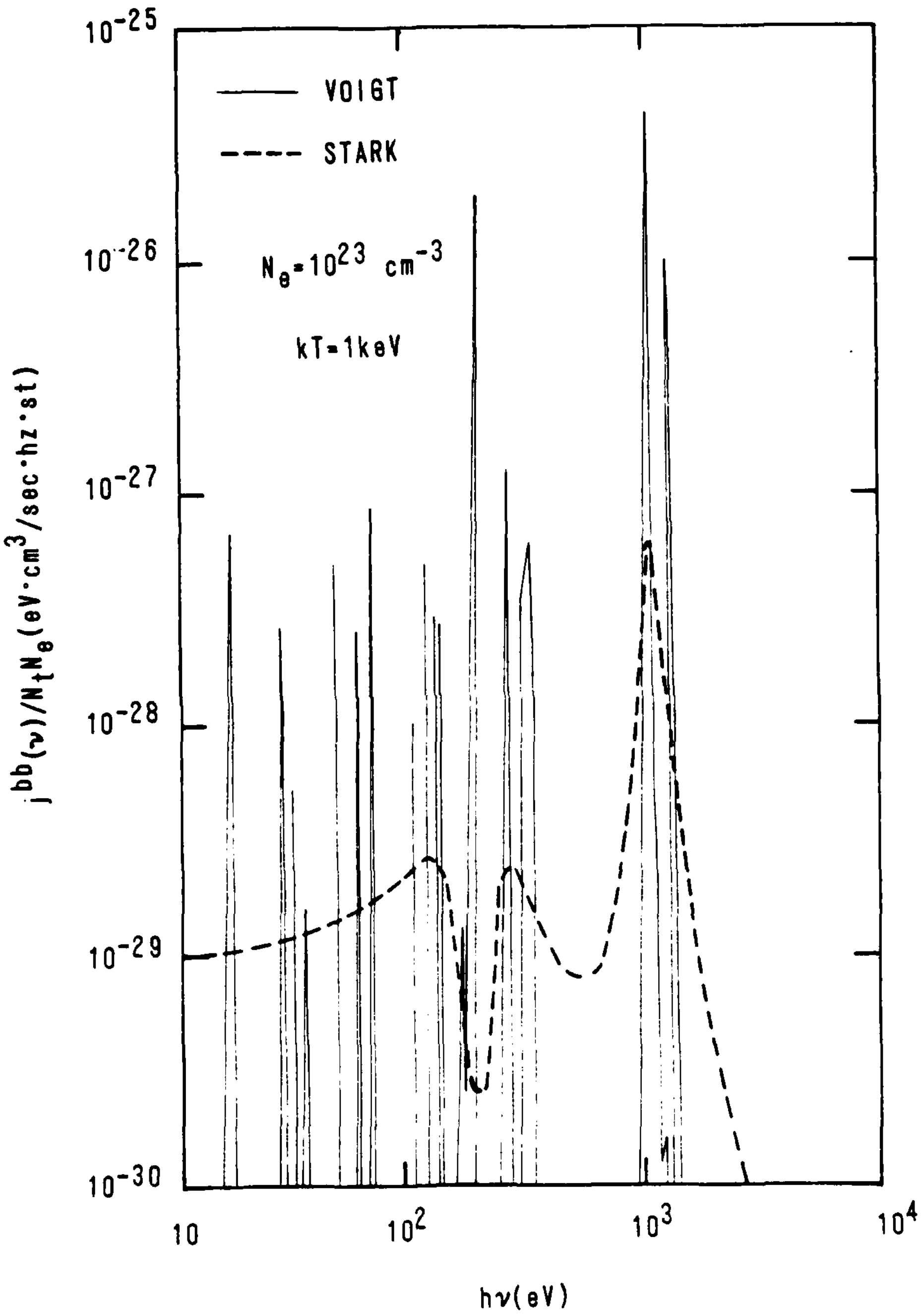

Fig. 7 - Comparison of bound-bound emission coefficients vs. frequency at kT = 1000 eV and $N_e = 10^{23}$ cm^{-3} for Voigt and Stark profiles.

III. LINE BROADENING

An effort is currently underway to develop methods to understand and predict the behavior of hot dense laboratory plasmas, in particular, those associated with, exploded wire, imploded microballoon and plasma wall interaction experiments. A key diagnostic tool for understanding the behavior of these hot gases is the emitted radiation. The emitted radiation depends on various absorption mechanisms within the plasma itself. Hence it becomes imperative to understand these absorption processes and be able to predict their magnitude in order to use the emission diagnostics as a guide for determining conditions within the plasma.

In this section we will discuss two related topics. The first is Stark broadening line profiles. Stark broadened line profiles for those whose frequency is in the optically thin window of the plasma, lead directly to a density diagnostic. In addition, the wings of the lines subject to linear Stark broadening are so wide that they contribute substantially to the overall opacity. For a range of temperatures and densities there are approximations, such as coronal equilibrium or LTE, which mitigate the need to solve the full set of detailed rate equations in order to find the distribution of excited state populations. In regions where these approximations are not justified one must resort to the solution of the rate equations. In addition, if the physical dimensions of the plasma are large enough self absorption of the radiation emitted within the plasma may have a substantial effect on the populations. Hence, our second topic concerns itself with collisional-radiative equilibrium, and our work on the radiation transport coupled with the collisional-radiative equilibrium.

A. Stark Broadened Line Profiles

A convenient diagnostic for the (electron) density in hot high density plasmas in the Stark broadened profiles of the lines emitted by one and two electron ions. These lines are often wide enough and sufficiently isolated to be resolved experimentally. By comparing to theoretical line profiles one can infer the electron density of the emitting plasma. Theoretical line profiles of lines emitted by the hydrogenic ions of C, O, Ne, Mg, Aℓ and Si (for the case where the perturbing and radiating ions are the same), were published recently (NRL Memorandum Report 3634, and Phys. Rev. 19, 2421 (1979)). However for the imploeded microballoon experiments one is often more interested in the density of the fuel (D,T). To measure this a small amount of high Z seed is added to the fuel. Now the perturbing ions are predominantly hydrogen (singly charged) and new profiles must be calculated using the electric microfield distribution appropriate to a mixture of perturbing ions with charge one (hydrogen) and Z-1 (where Z is the nuclear charge of the seed). In addition many of the experiments to date do not reach high enough temperatures for the seed ions to reach the hydrogenic state, although the helium-like state is substantially populated. For this reason it was desirable to have line profiles of the two electron ions. The computer program for the one electron line profiles was written using the parabolic coordinate representation to capitalize on the fact that H(f), the field dependent Hamiltonian, is diagonal in that representation. Unfortunately, the equivalent Hamiltonian for the two-electron ions is not diagonal for all values of f in any single representation. Thus we had not only to modify the subroutines that evaluate the relevant matrix elements, but rewrite the main program so as to transform to that

representation which diagonalizes H(f) for each value of f considered. To date we have only calculated two-electron profiles for Ne and Ar. These profiles were calculated using the microfield distributions for a mixture of singly and multiply charged perturbers. The microfield distributions we used were provided by Dr. C. Hooper. We used those for 10% seed and 90% hydrogen and $T_e = T_i$ for the one-and two-electron neon profiles, and the two-electron argon profiles. For the one-electron argon profiles we used the microfield distribution for a trace of argon in hydrogen.

The electric microfield distributions for mixtures change slowly with the mix-ratio so that an approximate ratio is adequate. Thus the microfield for 10% is close enough to that for a trace that either can be used for seeded microballoon experiments.

For the hydrogenic profiles, the strong collisions part of the electron impact broadening was obtained by fitting to the results of our distorted wave scattering calculations. This fitting was done for oxygen and aluminum. The results for neon are an interpolation and should be quite good. The results for argon are an extrapolation and are known to be slightly in error. For the two-electron profiles the strong collision part of the electron impact broadening was simply chosen to preserve the unitarity of the operator. The extension of the one-electron case to argon and a similar improvement (in the strong collision term) in the two-electron profiles is planned for the near future, however, the improvement is not expected to be large. Calculations for other ions and microfields will be amde one the above improvements have been implemented.

Since the theory predicts symmetry hydrogenic profiles, only one side is computed or tabulated. The structure of the two-electron system leads to non symmetric profiles. Thus we must compute both the red and blue sides of the line. The sensitivity of the profiles to the actual values of the umperturbed energy level is demonstrated best for Ne IX $1s3p - 1s^2$ where the 1s3s and 1s3d levels are closer to each other than either is to the 1s3p. This ordering of the levels leads to the surprising result that the lower density profiles have the two components further apart than the higher density cases. This is counter intuitive since it is a well known property of two-level Hermitian operators that the components repel each other with increasing strengths of the interactions (collisions).

To further illustrate the sensitivity of the profiles to the unpertured energy levels we arbitrarily changed the energy of the 1s3d level The change was an increase of about 0.2% (865 $\rightarrow$ 867) but is enough to bring the 1s3d level above the 1s3p. The results are included in the plots where it is labeled "E(ed" MOD". As can be seen, for densities $\sim 10^{23}$ the change is minimal but for 10^{22} the change is dramatic. Thus the need for accurate unperturbed energy levels for all angular momenta is critical if the line profiles are to be used at any but the highest densities.

Some of the energy levels used in the calculations were provided by R. D. Cowan, who is working on a set of self-consistent energy levels for Neon and Argon. The use of this self-consistant set of energy levels will reduce the uncertainty in some of the profiles and allow us to extend the calculations to other lines.

The line profiles are tabulated in Appendix I and plotted in Appendix II. In both cases the normalized line profiles are presented with the usual parameter alpha as the independent variable. The conversion from alpha to energy (in eV) is

$$E\ (\mathrm{eV}) = \alpha \left[\frac{10^{-8}\ F_o}{\lambda^2\ 8066}\right]$$

where $F_o = 2.61\ e\ N_e^{2/3} = 1.25 \times 10^{-9}\ N_e^{2/3}$, λ is in cm and N_e in cm^{-3}. The plots are included to assist in evaluating the need for interpolating between the plots for various densities. Thus for the case of Ar XVII 1s3p - 1s(2) the curves for 10^{23} and 5×10^{23} are so similar that interpolation is easy (and probably not even necessary) while between 10^{22} and 10^{23} (at least for negative alpha) the curves are sufficiently different to render interpolation difficult.

B. Collisional Radiative Equilibrium and Radiation Transport

A much larger correction to the line profiles (at least for the 1s2p - $1s^2$ and Lyman alpha) is opacity broadening. The radiation transport of the model where the emission/absorption profiles are Stark or convoluted Doppler and Stark profiles has already been demonstrated for the case of an aluminum cylindrical plasma (Bull. Am. Phys. Soc. 23, (1978) No. 6E10). The merging of lines to other lines and/or the continuum has also been demonstrated, this time in a planar aluminum model (Bull. Am. Phys. Soc. 24, 1054, (1979) No. 705). The techniques for handling these problems are known, it does remain to implement them in one common code. Our radiation transport-collisional radiative equilibrium

code is being changed to accept a standard format for the atomic data. The rates etc. for neon, aluminum, titanium and argon models have been generated and/or collected in the new format. In the near future we will test the improved radiation transport code.

As the density goes even higher ($N > 10^{24}$) the energy levels predicted for isolated atoms/ions are shifted by the free charges in the vicinity of the atom/ion. There have been many calculations of these changes, but so far few, if any, are self consistent. There are techniques for the calculations of self consistent potentials and therefore the energy levels in these potentials. (Phys. Rev. L, 957, (1070). We will utilize these techniques to try to find shifts in energy levels, continuum edges and collisional rates for atoms/ions at these very high densities.

These shifts are not only of diagnostic importance but can alter the opacity and thus the equation of state.

APPENDIX I

NEON IX 1S2P - 1S(2), T = 4.0E6 (DEG. K)

	1.00E 22	1.00E 23
-1.00E-08	1.15E 06	2.81E 06
-7.00E-09	2.19E 06	4.73E 06
-5.00E-09	4.00E 06	7.71E 06
-3.00E-09	9.88E 06	1.63E 07
-2.00E-09	1.99E 07	2.93E 07
-1.50E-09	3.21E 07	4.33E 07
-1.00E-09	6.03E 07	7.04E 07
-7.00E-10	9.92E 07	9.98E 07
-5.00E-10	1.48E 08	1.29E 08
-3.00E-10	2.37E 08	1.68E 08
-1.00E-10	3.92E 08	2.18E 08
-7.00E-11	4.21E 08	2.26E 08
-5.00E-11	4.40E 08	2.31E 08
-3.00E-11	4.60E 08	2.37E 08
-2.00E-11	4.69E 08	2.39E 08
-1.00E-11	4.79E 08	2.42E 08
-3.00E-12	4.86E 08	2.44E 08
0.00E 00	4.88E 08	2.44E 08
3.00E-12	4.91E 08	2.45E 08
1.00E-11	4.98E 08	2.47E 08
2.00E-11	5.07E 08	2.50E 08
3.00E-11	5.15E 08	2.52E 08
5.00E-11	5.32E 08	2.57E 08
7.00E-11	5.47E 08	2.62E 08
1.00E-10	5.66E 08	2.70E 08
3.00E-10	5.42E 08	3.02E 08
5.00E-10	3.86E 08	2.97E 08
7.00E-10	2.70E 08	2.59E 08
1.00E-09	1.77E 08	1.90E 08
1.50E-09	1.08E 08	1.16E 08
2.00E-09	7.29E 07	8.09E 07
3.00E-09	3.92E 07	5.00E 07
5.00E-09	1.60E 07	2.68E 07
7.00E-09	8.35E 06	1.65E 07
1.00E-08	4.05E 06	8.97E 06

NEON IX 1S3P - 1S(2), T = 4.0E6 (DEG. K)

	1.00E 22	1.00E 23
-1.00E-07	6.51E 05	4.02E 05
-8.00E-08	1.26E 06	7.32E 05
-6.00E-08	2.68E 06	1.54E 06
-5.00E-08	3.85E 06	2.38E 06
-4.00E-08	5.21E 06	3.84E 06
-3.50E-08	5.54E 06	4.93E 06
-3.00E-08	3.92E 06	6.34E 06
-2.50E-08	8.53E 05	8.11E 06
-2.00E-08	8.08E 05	1.00E 07
-1.50E-08	1.12E 06	1.11E 07
-1.00E-08	1.85E 06	8.77E 06
-5.00E-09	3.75E 06	3.61E 06
0.00E 00	1.08E 07	4.74E 06
5.00E-09	2.53E 07	1.12E 07
1.00E-08	2.46E 07	1.75E 07
1.50E-08	1.83E 07	1.73E 07
2.00E-08	1.30E 07	1.40E 07
2.50E-08	9.41E 06	1.06E 07
3.00E-08	6.91E 06	7.97E 06
3.50E-08	5.17E 06	6.01E 06
4.00E-08	3.96E 06	4.59E 06
5.00E-08	2.44E 06	2.77E 06
6.00E-08	1.58E 06	1.75E 06
8.00E-08	7.71E 05	8.11E 05
1.00E-07	4.30E 05	4.39E 05

NECN IX 1S3P - 1S(2), E(3D) MOD.

	1.00E 22	1.00E 23
-1.00E-07	5.41E 05	3.88E 05
-8.00E-08	1.01E 06	6.99E 05
-6.00E-08	1.97E 06	1.45E 06
-5.00E-08	2.62E 06	2.21E 06
-4.00E-08	2.94E 06	3.51E 06
-3.50E-08	3.13E 06	4.47E 06
-3.00E-08	3.84E 06	5.72E 06
-2.50E-08	5.26E 06	7.36E 06
-2.00E-08	7.59E 06	9.46E 06
-1.50E-08	1.12E 07	1.20E 07
-1.00E-08	1.61E 07	1.41E 07
-5.00E-09	2.06E 07	1.34E 07
-3.00E-09	2.16E 07	1.18E 07
-2.00E-09	2.20E 07	1.08E 07
-1.00E-09	2.25E 07	9.67E 06
0.00E 00	2.29E 07	8.52E 06
5.00E-10	2.27E 07	7.94E 06
1.00E-09	2.21E 07	7.36E 06
1.50E-09	2.09E 07	6.78E 06
2.00E-09	1.92E 07	6.21E 06
2.50E-09	1.71E 07	5.66E 06
3.00E-09	1.50E 07	5.15E 06
4.00E-09	1.11E 07	4.40E 06
5.00E-09	8.23E 06	4.13E 06
7.00E-09	4.81E 06	5.21E 06
1.00E-08	2.55E 06	8.93E 06
1.50E-08	1.37E 06	1.37E 07
2.00E-08	3.06E 06	1.36E 07
2.50E-08	8.23E 06	1.12E 07
3.00E-08	9.17E 06	8.68E 06
3.50E-08	7.87E 06	6.59E 06
4.00E-08	6.24E 06	5.01E 06
5.00E-08	3.73E 06	2.98E 06
6.00E-08	2.30E 06	1.87E 06
8.00E-08	1.01E 06	8.50E 05
1.00E-07	5.30E 05	4.54E 05

NEON X L_α, T = 4.0 E6 (DEG. K)

	1.00E 22	1.00E 23	5.00E 23
0.00E 00	5.21E 08	3.17E 08	2.41E 08
3.00E-11	5.18E 08	3.16E 08	2.41E 08
1.00E-10	4.90E 08	3.10E 08	2.38E 08
3.00E-10	3.30E 08	2.63E 08	2.17E 08
5.00E-10	2.00E 08	2.03E 08	1.85E 08
7.00E-10	1.27E 08	1.52E 08	1.52E 08
1.00E-09	7.19E 07	9.96E 07	1.12E 08
1.50E-09	3.62E 07	5.61E 07	7.00E 07
2.00E-09	2.27E 07	3.68E 07	4.83E 07
3.00E-09	1.34E 07	2.20E 07	2.96E 07
5.00E-09	1.04E 07	1.52E 07	1.91E 07
7.00E-09	1.05E 07	1.32E 07	1.48E 07
1.00E-08	9.65E 06	1.01E 07	9.86E 06
1.50E-08	6.16E 06	5.28E 06	4.56E 06
2.00E-08	3.45E 06	2.73E 06	2.23E 06
2.50E-08	1.97E 06	1.50E 06	1.20E 06
3.00E-08	1.19E 06	8.90E 05	7.14E 05
3.50E-08	7.71E 05	5.68E 05	4.56E 05
4.00E-08	5.22E 05	3.83E 05	3.13E 05
4.50E-08	3.80E 05	2.72E 05	2.27E 05
5.00E-08	2.68E 05	1.98E 05	1.68E 05
6.00E-08	1.58E 05	1.18E 05	9.67E 04
7.00E-08	1.02E 05	7.77E 04	5.43E 04
1.00E-07	3.66E 04	3.13E 04	6.28E 03

NECN X L_ρ , T = 4.0 E6 (DEG. K)

	1.00E 22	1.00E 23	5.00E 23
0.00E 00	3.20E 06	5.84E 06	8.52E 06
3.00E-11	3.20E 06	5.84E 06	8.52E 06
1.00E-10	3.20E 06	5.85E 06	8.53E 06
3.00E-10	3.25E 06	5.91E 06	8.62E 06
5.00E-10	3.35E 06	6.03E 06	8.78E 06
7.00E-10	3.48E 06	6.20E 06	9.03E 06
1.00E-09	3.75E 06	6.56E 06	9.52E 06
1.50E-09	4.41E 06	7.38E 06	1.06E 07
2.00E-09	5.23E 06	8.48E 06	1.21E 07
3.00E-09	7.21E 06	1.10E 07	1.53E 07
5.00E-09	1.18E 07	1.60E 07	2.08E 07
7.00E-09	1.57E 07	1.94E 07	2.33E 07
1.00E-08	1.83E 07	2.02E 07	2.20E 07
1.20E-08	1.80E 07	1.88E 07	1.94E 07
1.40E-08	1.68E 07	1.68E 07	1.66E 07
1.50E-08	1.60E 07	1.57E 07	1.53E 07
1.60E-08	1.51E 07	1.46E 07	1.40E 07
1.80E-08	1.33E 07	1.26E 07	1.17E 07
2.00E-08	1.17E 07	1.08E 07	9.82E 06
2.20E-08	1.03E 07	9.25E 06	8.25E 06
2.50E-08	8.38E 06	7.37E 06	6.39E 06
3.00E-08	6.03E 06	5.10E 06	4.25E 06
3.50E-08	4.36E 06	3.57E 06	2.89E 06
4.00E-08	3.22E 06	2.57E 06	2.03E 06
4.50E-08	2.41E 06	1.89E 06	1.48E 06
5.00E-08	1.83E 06	1.42E 06	1.10E 06
6.00E-08	1.12E 06	8.54E 05	6.48E 05
7.00E-08	7.33E 05	5.52E 05	3.99E 05
1.00E-07	2.63E 05	1.99E 05	1.13E 05

NEON X Lγ, T = 4.0E6 (DEG. K)

	1.00E 22	1.00E 23
0.00E 00	2.46E 07	2.36E 07
3.00E-11	2.46E 07	2.36E 07
1.00E-10	2.46E 07	2.36E 07
3.00E-10	2.44E 07	2.35E 07
5.00E-10	2.41E 07	2.33E 07
7.00E-10	2.37E 07	2.29E 07
1.00E-09	2.29E 07	2.22E 07
1.50E-09	2.10E 07	2.07E 07
2.00E-09	1.89E 07	1.90E 07
2.50E-09	1.69E 07	1.72E 07
3.00E-09	1.49E 07	1.55E 07
4.00E-09	1.18E 07	1.27E 07
5.00E-09	9.55E 06	1.07E 07
7.00E-09	7.03E 06	8.39E 06
1.00E-08	5.75E 06	7.32E 06
1.50E-08	5.75E 06	7.42E 06
2.00E-08	6.14E 06	7.54E 06
2.50E-08	6.23E 06	7.16E 06
3.00E-08	5.97E 06	6.41E 06
3.50E-08	5.47E 06	5.53E 06
4.00E-08	4.83E 06	4.63E 06
4.50E-08	4.21E 06	3.86E 06
5.00E-08	3.63E 06	3.19E 06
6.00E-08	2.62E 06	2.16E 06
7.00E-08	1.91E 06	1.50E 06
8.00E-08	1.40E 06	1.06E 06
9.00E-08	1.04E 06	7.67E 05
1.00E-07	7.91E 05	5.69E 05
2.00E-07	1.12E 05	7.33E 04
3.00E-07	3.42E 04	2.43E 04

NEON X Lδ, T = 4.0E6 (DEG. K)

	1.00E 22
0.00E 00	3.07E 06
1.00E-09	3.12E 06
3.00E-09	3.46E 06
7.00E-09	4.76E 06
1.00E-08	5.74E 06
1.50E-08	6.62E 06
2.00E-08	6.54E 06
2.50E-08	6.01E 06
3.00E-08	5.41E 06
4.00E-08	4.47E 06
5.00E-08	3.77E 06
7.00E-08	2.63E 06
1.00E-07	1.43E 06
2.00E-07	2.44E 05
3.00E-07	7.51E 04
5.00E-07	1.68E 04
7.00E-07	5.23E 03
1.00E-06	2.29E 03

ARGON XVII 1S2P - 1S(2), T =4.63E6 (DEG. K)

	1.00E 23	5.00E 23
-1.00E-09	4.93E 06	7.64E 06
-8.00E-10	7.58E 06	1.07E 07
-5.00E-10	1.86E 07	2.42E 07
-3.00E-10	4.89E 07	6.09E 07
-2.50E-10	6.87E 07	8.45E 07
-2.00E-10	1.04E 08	1.25E 08
-1.50E-10	1.75E 08	2.07E 08
-1.00E-10	3.57E 08	4.07E 08
-5.00E-11	1.11E 09	1.15E 09
-7.00E-11	6.53E 08	7.12E 08
-2.00E-11	3.63E 09	3.14E 09
-1.00E-11	6.27E 09	4.82E 09
0.00E 00	1.08E 10	7.42E 09
1.00E-11	1.33E 10	9.93E 09
2.00E-11	9.88E 09	9.55E 09
5.00E-11	3.57E 09	3.81E 09
7.00E-11	2.37E 09	2.51E 09
1.00E-10	1.46E 09	1.65E 09
1.50E-10	7.73E 08	9.78E 08
2.00E-10	4.56E 08	6.31E 08
2.50E-10	2.95E 08	4.32E 08
3.00E-10	2.01E 08	3.05E 08
5.00E-10	6.35E 07	9.83E 07
8.00E-10	2.07E 07	2.96E 07
1.00E-09	1.19E 07	1.62E 07

ARGON XVII 1S2P - 1S(2), T = 9.3E6 (DEG. K)

	1.00E 23	5.00E 23
-1.00E-09	4.10E 06	6.76E 06
-8.00E-10	6.28E 06	9.32E 06
-5.00E-10	1.54E 07	2.09E 07
-3.00E-10	4.03E 07	5.25E 07
-2.50E-10	5.67E 07	7.30E 07
-2.00E-10	8.58E 07	1.09E 08
-1.50E-10	1.46E 08	1.82E 08
-1.00E-10	3.03E 08	3.67E 08
-5.00E-11	9.53E 08	1.11E 09
-7.00E-11	5.66E 08	6.60E 08
-2.00E-11	3.64E 09	3.36E 09
-1.00E-11	6.86E 09	5.44E 09
0.00E 00	1.28E 10	8.67E 09
1.00E-11	1.38E 10	1.07E 10
2.00E-11	8.38E 09	8.61E 09
5.00E-11	2.86E 09	2.78E 09
7.00E-11	2.01E 09	1.82E 09
1.00E-10	1.35E 09	1.26E 09
1.50E-10	7.92E 08	8.65E 08
2.00E-10	5.04E 08	6.40E 08
2.50E-10	3.51E 08	4.87E 08
3.00E-10	2.53E 08	3.77E 08
5.00E-10	9.55E 07	1.54E 08
8.00E-10	3.66E 07	5.44E 07
1.00E-09	2.19E 07	3.10E 07

ARGON XVII 1S3P - 1S(2), T = 4.6E6 (DEG. K)

	1.00E 23	5.00E 23
-1.00E-08	5.19E 05	4.81E 05
-9.00E-09	6.86E 05	6.10E 05
-8.00E-09	9.39E 05	7.92E 05
-7.00E-09	1.36E 06	1.07E 06
-6.00E-09	2.20E 06	1.56E 06
-5.00E-09	4.00E 06	2.47E 06
-3.00E-09	2.31E 07	1.09E 07
-2.50E-09	3.99E 07	1.92E 07
-2.00E-09	6.28E 07	3.72E 07
-1.70E-09	6.93E 07	5.76E 07
-1.50E-09	7.06E 07	7.81E 07
-1.20E-09	1.04E 08	1.25E 08
-1.00E-09	1.54E 08	1.70E 08
-7.00E-10	2.73E 08	2.72E 08
-5.00E-10	3.91E 08	3.61E 08
-3.00E-10	3.16E 08	4.05E 08
-1.00E-10	7.47E 07	2.52E 08
0.00E 00	7.90E 07	1.23E 08
1.00E-10	1.59E 08	1.59E 08
3.00E-10	4.36E 08	4.85E 08
5.00E-10	5.26E 08	5.85E 08
7.00E-10	4.40E 08	4.54E 08
1.00E-09	2.71E 08	2.53E 08
1.50E-09	1.13E 08	9.57E 07
2.00E-09	5.23E 07	4.16E 07
3.00E-09	1.55E 07	1.18E 07
5.00E-09	3.22E 06	2.64E 06
8.00E-09	8.84E 05	8.32E 05

ARGON XVII 1S3P - 1S(2), T = 9.3E6 (DEG. K)

	1.00E 22	1.00E 23	5.00E 23
-8.00E-09	8.42E 06	1.79E 06	1.14E 06
-5.00E-09	3.95E 06	7.83E 06	4.38E 06
-3.00E-09	2.08E 07	3.45E 07	2.09E 07
-2.50E-09	3.84E 07	5.36E 07	3.52E 07
-2.00E-09	8.00E 07	7.50E 07	6.24E 07
-1.70E-09	1.20E 08	8.04E 07	8.90E 07
-1.50E-09	1.54E 08	8.73E 07	1.13E 08
-1.20E-09	2.18E 08	1.28E 08	1.62E 08
-1.00E-09	2.91E 08	1.77E 08	2.06E 08
-7.00E-10	1.15E 08	2.67E 08	2.87E 08
-5.00E-10	1.40E 07	3.43E 08	3.19E 08
-3.00E-10	1.41E 07	1.92E 08	2.68E 08
-1.00E-10	3.38E 07	4.04E 07	1.31E 08
0.00E 00	7.54E 07	4.59E 07	6.85E 07
1.00E-10	2.05E 08	9.19E 07	9.40E 07
3.00E-10	4.74E 08	2.82E 08	2.83E 08
5.00E-10	4.96E 08	4.10E 08	4.18E 08
7.00E-10	4.03E 08	3.94E 08	4.04E 08
1.00E-09	2.57E 08	2.80E 08	2.83E 08
1.50E-09	1.35E 08	1.40E 08	1.35E 08
2.00E-09	8.00E 07	7.46E 07	6.74E 07
3.00E-09	2.85E 07	2.66E 07	2.13E 07
5.00E-09	7.52E 06	6.19E 06	4.44E 06
8.00E-09	2.39E 06	1.65E 06	1.15E 06

ARGON XVII 1S4P - 1S(2), T = 4.6E6 (DEG. K)

	1.00E 23	5.00E 23
-1.00E-08	1.71E 06	1.24E 06
-9.00E-09	2.30E 06	1.60E 06
-8.00E-09	3.23E 06	2.14E 06
-7.00E-09	4.79E 06	3.03E 06
-6.00E-09	7.56E 06	4.60E 06
-5.00E-09	1.28E 07	7.66E 06
-3.00E-09	4.57E 07	3.02E 07
-2.50E-09	6.37E 07	4.58E 07
-2.00E-09	8.65E 07	7.01E 07
-1.70E-09	1.01E 08	9.00E 07
-1.50E-09	1.09E 08	1.05E 08
-1.20E-09	1.18E 08	1.28E 08
-1.00E-09	1.19E 08	1.42E 08
-7.00E-10	1.10E 08	1.52E 08
-5.00E-10	1.04E 08	1.50E 08
-3.00E-10	1.12E 08	1.49E 08
-2.00E-10	1.34E 08	1.59E 08
-1.00E-10	1.86E 08	1.90E 08
0.00E 00	2.94E 08	2.65E 08
1.00E-10	4.47E 08	4.03E 08
2.00E-10	4.59E 08	4.93E 08
3.00E-10	3.19E 08	3.88E 08
4.00E-10	2.17E 08	2.63E 08
5.00E-10	1.68E 08	2.01E 08
7.00E-10	1.41E 08	1.77E 08
1.00E-09	1.47E 08	1.93E 08
1.50E-09	1.46E 08	1.76E 08
2.00E-09	1.19E 08	1.25E 08
3.00E-09	6.07E 07	5.18E 07
4.00E-09	2.99E 07	2.25E 07
5.00E-09	1.57E 07	1.12E 07
6.00E-09	8.98E 06	6.28E 06
7.00E-09	5.55E 06	3.92E 06
8.00E-09	3.68E 06	2.66E 06
9.00E-09	2.58E 06	1.92E 06
1.00E-08	1.89E 06	1.46E 06

ARGON XVII 1S4P - 1S(2), T = 9.3E6 (DEG. K)

	1.00E 23	5.00E 23
-1.00E-08	3.06E 06	2.07E 06
-9.00E-09	4.13E 06	2.77E 06
-8.00E-09	5.76E 06	3.85E 06
-7.00E-09	8.31E 06	5.62E 06
-6.00E-09	1.24E 07	8.67E 06
-5.00E-09	1.96E 07	1.43E 07
-3.00E-09	5.50E 07	4.69E 07
-2.50E-09	7.08E 07	6.40E 07
-2.00E-09	8.76E 07	8.54E 07
-1.70E-09	9.55E 07	9.86E 07
-1.50E-09	9.84E 07	1.06E 08
-1.20E-09	9.73E 07	1.14E 08
-1.00E-09	9.17E 07	1.15E 08
-7.00E-10	7.92E 07	1.10E 08
-5.00E-10	7.63E 07	1.06E 08
-3.00E-10	9.64E 07	1.18E 08
-2.00E-10	1.30E 08	1.39E 08
-1.00E-10	2.01E 08	1.86E 08
0.00E 00	3.38E 08	2.72E 08
1.00E-10	4.83E 08	3.87E 08
2.00E-10	4.11E 08	4.11E 08
3.00E-10	2.58E 08	3.09E 08
4.00E-10	1.70E 08	2.13E 08
5.00E-10	1.29E 08	1.58E 08
7.00E-10	1.02E 08	1.23E 08
1.00E-09	1.06E 08	1.26E 08
1.50E-09	1.18E 08	1.36E 08
2.00E-09	1.08E 08	1.18E 08
3.00E-09	6.58E 07	6.71E 07
4.00E-09	3.74E 07	3.50E 07
5.00E-09	2.21E 07	1.91E 07
6.00E-09	1.38E 07	1.12E 07
7.00E-09	9.08E 06	7.00E 06
8.00E-09	6.22E 06	4.67E 06
9.00E-09	4.43E 06	3.28E 06
1.00E-08	3.26E 06	2.40E 06

ARGON XVIII L_α , T = 9.3E6 (DEG. K)

	1.00E 22	1.00E 23	5.00E 23
0.00E 00	2.27E 10	1.29E 10	9.00E 09
3.00E-12	2.04E 10	1.24E 10	8.85E 09
1.00E-11	1.02E 10	9.28E 09	7.60E 09
3.00E-11	1.91E 09	2.90E 09	3.41E 09
5.00E-11	7.50E 08	1.25E 09	1.67E 09
7.00E-11	4.15E 08	7.08E 08	9.84E 08
1.00E-10	2.44E 08	4.10E 08	5.78E 08
1.50E-10	1.78E 08	2.71E 08	3.70E 08
2.00E-10	1.79E 08	2.46E 08	3.18E 08
3.00E-10	2.16E 08	2.56E 08	2.95E 08
5.00E-10	2.09E 08	2.12E 08	2.10E 08
7.00E-10	1.36E 08	1.26E 08	1.15E 08
1.00E-09	5.83E 07	5.14E 07	4.44E 07
1.50E-09	1.80E 07	1.56E 07	1.33E 07
2.00E-09	7.84E 06	6.65E 06	5.65E 06
2.50E-09	4.06E 06	3.31E 06	2.88E 06
3.00E-09	2.58E 06	1.91E 06	1.67E 06
3.50E-09	1.87E 06	1.24E 06	1.06E 06
4.00E-09	1.41E 06	8.48E 05	7.07E 05
4.50E-09	1.08E 06	6.15E 05	5.00E 05
5.00E-09	8.61E 05	4.75E 05	3.75E 05
6.00E-09	5.36E 05	2.91E 05	2.27E 05
7.00E-09	3.66E 05	1.96E 05	1.53E 05

ARGON XVIII L_β , T = 9.3E6 (DEG. K)

	1.00E 22	1.00E 23	5.00E 23
0.00E 00	4.15E 07	7.39E 07	1.08E 08
1.00E-11	4.22E 07	7.47E 07	1.09E 08
3.00E-11	4.76E 07	8.06E 07	1.15E 08
5.00E-11	5.85E 07	9.20E 07	1.28E 08
7.00E-11	7.21E 07	1.08E 08	1.46E 08
1.00E-10	9.87E 07	1.38E 08	1.79E 08
1.20E-10	1.20E 08	1.60E 08	2.04E 08
1.50E-10	1.55E 08	1.98E 08	2.45E 08
1.70E-10	1.81E 08	2.24E 08	2.72E 08
2.00E-10	2.20E 08	2.65E 08	3.14E 08
2.50E-10	2.85E 08	3.29E 08	3.78E 08
3.00E-10	3.42E 08	3.83E 08	4.27E 08
5.00E-10	4.35E 08	4.48E 08	4.60E 08
8.00E-10	3.17E 08	3.09E 08	2.99E 08
1.00E-09	2.29E 08	2.20E 08	2.08E 08
1.50E-09	1.06E 08	9.88E 07	8.96E 07
2.00E-09	5.24E 07	4.76E 07	4.21E 07
2.50E-09	2.85E 07	2.55E 07	2.24E 07
3.00E-09	1.72E 07	1.49E 07	1.31E 07
4.00E-09	8.08E 06	6.53E 06	5.64E 06
5.00E-09	4.65E 06	3.49E 06	2.96E 06
7.00E-09	2.01E 06	1.35E 06	1.11E 06
1.00E-09	8.61E 05	6.75E 05	6.06E 05

ARGON XVIII $L\gamma$, T = 9.3E6 (DEG. K)

	1.00E 22	1.00E 23	5.00E 23
0.00E 00	8.26E 08	5.92E 08	5.46E 08
1.00E-11	8.18E 08	5.90E 08	5.44E 08
3.00E-11	7.62E 08	5.70E 08	5.30E 08
5.00E-11	6.69E 08	5.34E 08	5.03E 08
7.00E-11	5.68E 08	4.89E 08	4.68E 08
1.00E-10	4.32E 08	4.16E 08	4.10E 08
1.20E-10	3.61E 08	3.70E 08	3.72E 08
1.50E-10	2.80E 08	3.11E 08	3.21E 08
1.70E-10	2.41E 08	2.78E 08	2.91E 08
2.00E-10	1.97E 08	2.39E 08	2.55E 08
2.50E-10	1.53E 08	1.93E 08	2.12E 08
3.00E-10	1.28E 08	1.64E 08	1.84E 08
5.00E-10	1.09E 08	1.33E 08	1.54E 08
8.00E-10	1.30E 08	1.46E 08	1.65E 08
1.00E-09	1.40E 08	1.52E 08	1.67E 08
1.50E-09	1.31E 08	1.34E 08	1.36E 08
2.00E-09	9.85E 07	9.64E 07	9.23E 07
2.50E-09	6.80E 07	6.48E 07	5.95E 07
3.00E-09	4.62E 07	4.33E 07	3.86E 07
4.00E-09	2.23E 07	2.05E 07	1.77E 07
5.00E-09	1.21E 07	1.10E 07	9.29E 06
7.00E-09	4.79E 06	4.19E 06	3.43E 06
1.00E-08	1.95E 06	1.49E 06	1.16E 06

ARGON XVIII L_δ , T = 9.3E6 (DEG. K)

	1.00E 22	1.00E 23	5.00E 23
0.00E 00	5.60E 07	7.30E 07	8.05E 07
1.00E-11	5.60E 07	7.30E 07	8.06E 07
3.00E-11	5.65E 07	7.35E 07	8.13E 07
5.00E-11	5.74E 07	7.45E 07	8.28E 07
7.00E-11	5.88E 07	7.59E 07	8.49E 07
1.00E-10	6.16E 07	7.88E 07	8.92E 07
1.20E-10	6.40E 07	8.13E 07	9.27E 07
1.50E-10	6.81E 07	8.56E 07	9.89E 07
1.70E-10	7.13E 07	8.88E 07	1.04E 08
2.00E-10	7.64E 07	9.41E 07	1.11E 08
2.50E-10	8.62E 07	1.04E 08	1.25E 08
3.00E-10	9.67E 07	1.14E 08	1.38E 08
5.00E-10	1.35E 08	1.50E 08	1.80E 08
8.00E-10	1.54E 08	1.61E 08	1.80E 08
1.00E-09	1.45E 08	1.50E 08	1.61E 08
1.50E-09	1.12E 08	1.16E 08	1.22E 08
2.00E-09	9.20E 07	9.48E 07	9.81E 07
2.50E-09	7.73E 07	7.82E 07	7.79E 07
3.00E-09	6.39E 07	6.29E 07	6.00E 07
4.00E-09	4.09E 07	3.83E 07	3.37E 07
5.00E-09	2.55E 07	2.30E 07	1.89E 07
7.00E-09	1.10E 07	9.33E 06	7.14E 06
1.00E-08	4.14E 06	3.33E 06	2.40E 06

APPENDIX II

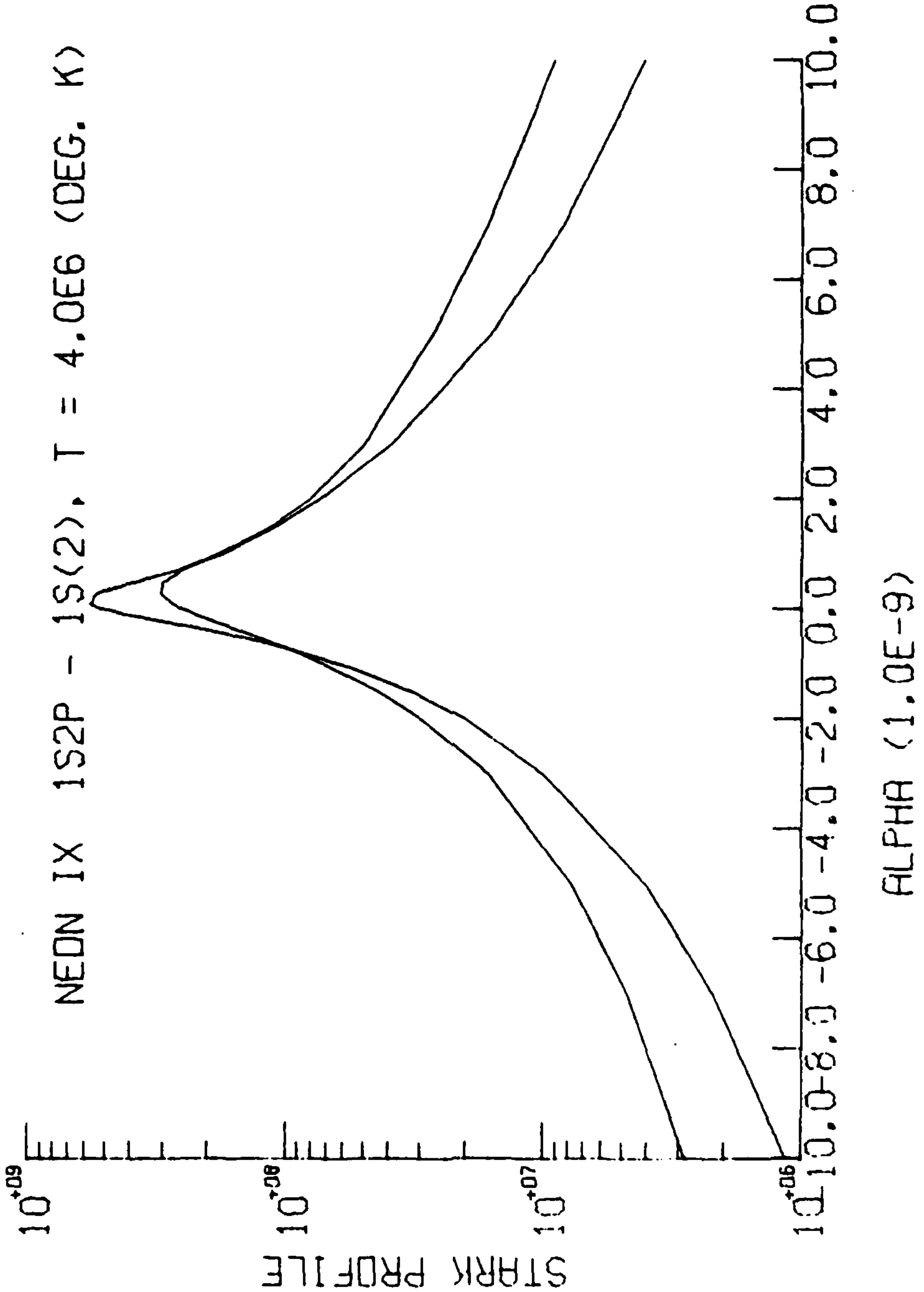
NEON IX 1S2P - 1S(2), T = 4.0E6 (DEG. K)
ALPHA (1.0E-9)
STARK PROFILE
-10.0 -8.0 -6.0 -4.0 -2.0 0.0 2.0 4.0 6.0 8.0 10.0
10^{+06} 10^{+07} 10^{+08} 10^{+09}

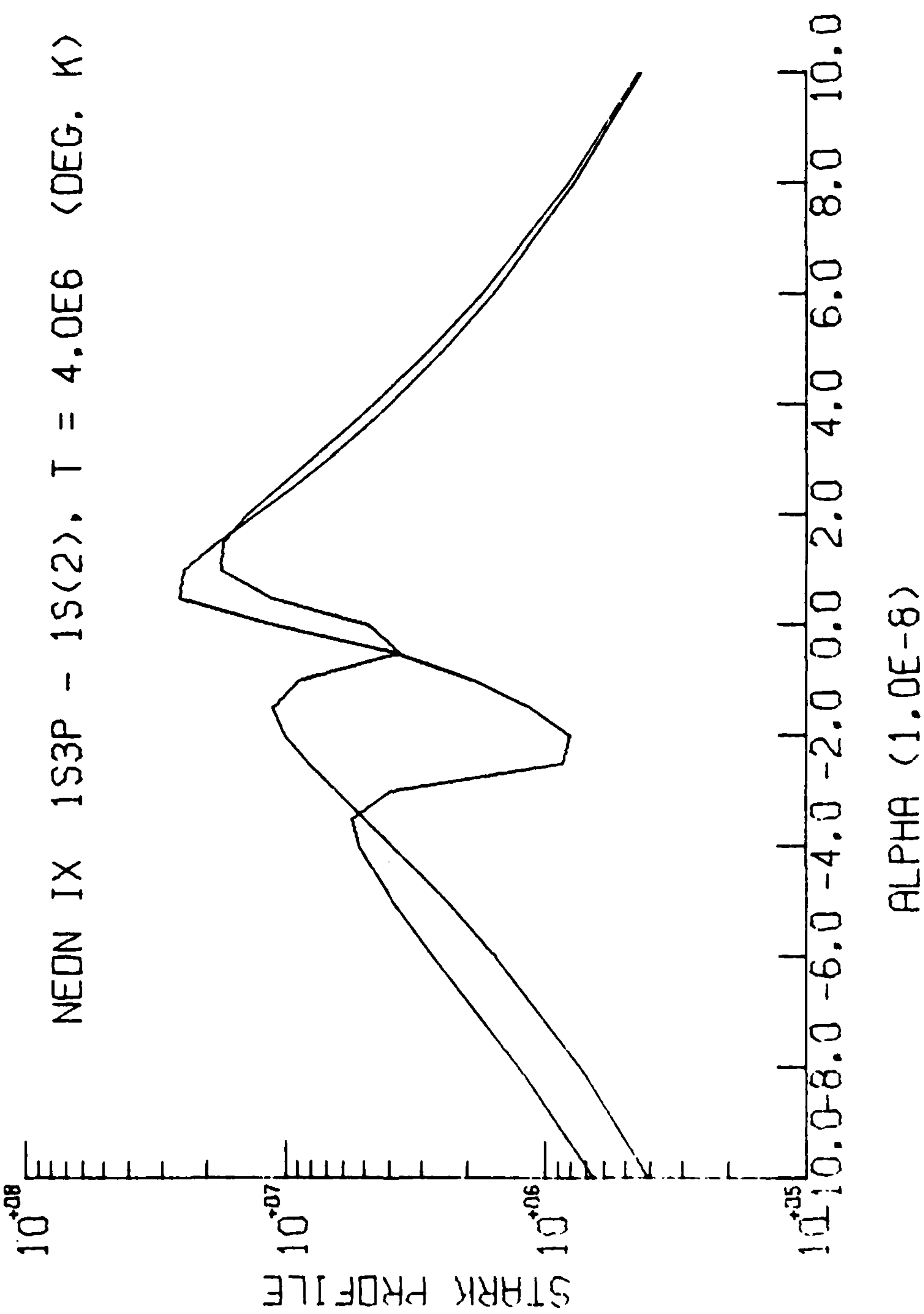
NEON IX 1S3P - 1S(2), T = 4.0E6 (DEG. K)
STARK PROFILE
ALPHA (1.0E-8)
10.0
8.0
6.0
4.0
2.0
0.0
-2.0
-4.0
-6.0
-8.0
-10.0
10^{+08}
10^{+07}
10^{+06}
10^{+05}

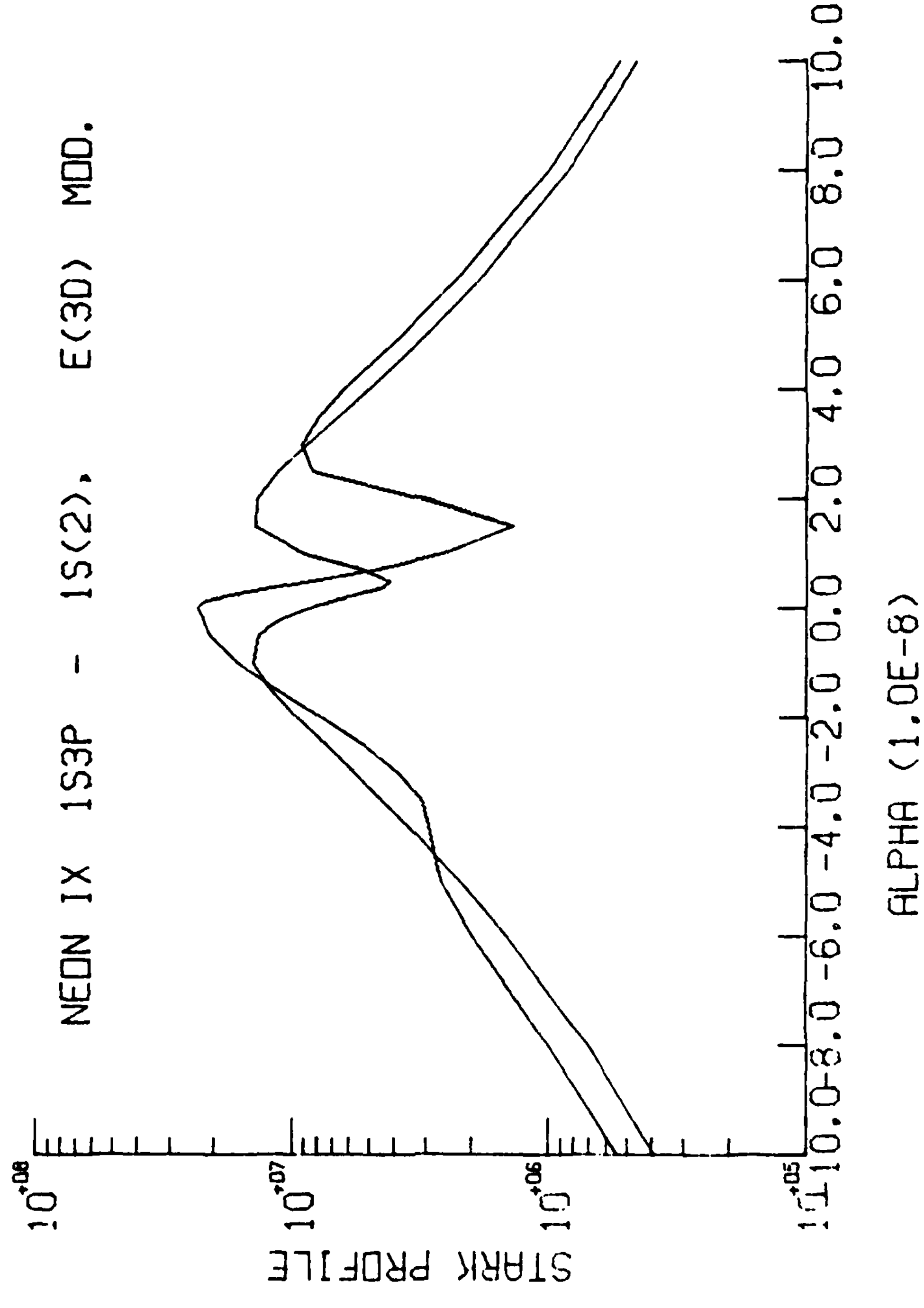

NEON IX 1S3P - 1S(2), E(3D) MOD.
STARK PROFILE
ALPHA (1.0E-8)
-10.0
-8.0
-6.0
-4.0
-2.0
0.0
2.0
4.0
6.0
8.0
10.0
10^{+08}
10^{+07}
10^{+06}
10^{+05}

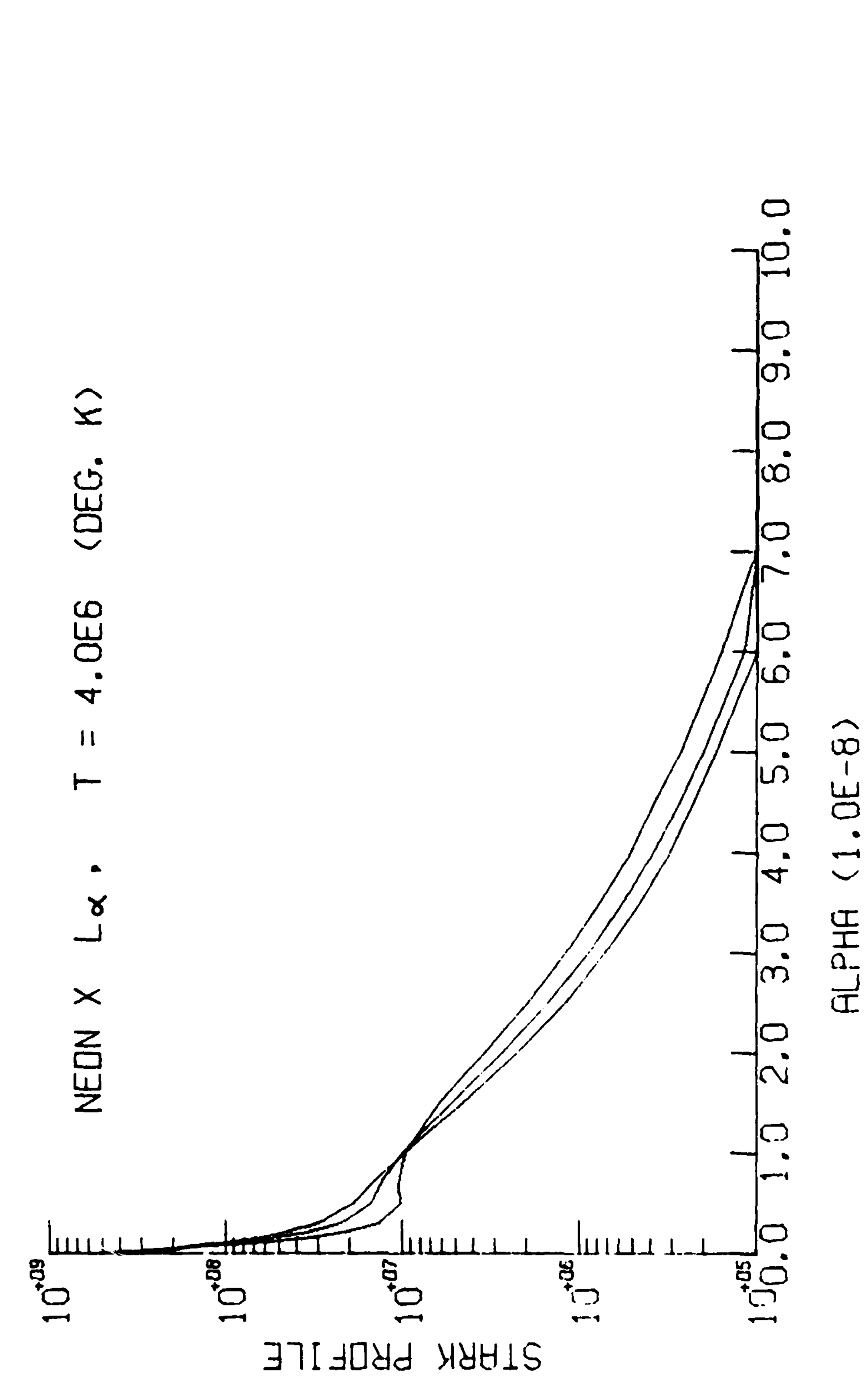

NEON X Lα, T = 4.0E6 (DEG. K)
STARK PROFILE
ALPHA (1.0E-8)
10^{+09}
10^{+08}
10^{+07}
10^{+06}
10^{+05}
0.0
1.0
2.0
3.0
4.0
5.0
6.0
7.0
8.0
9.0
10.0

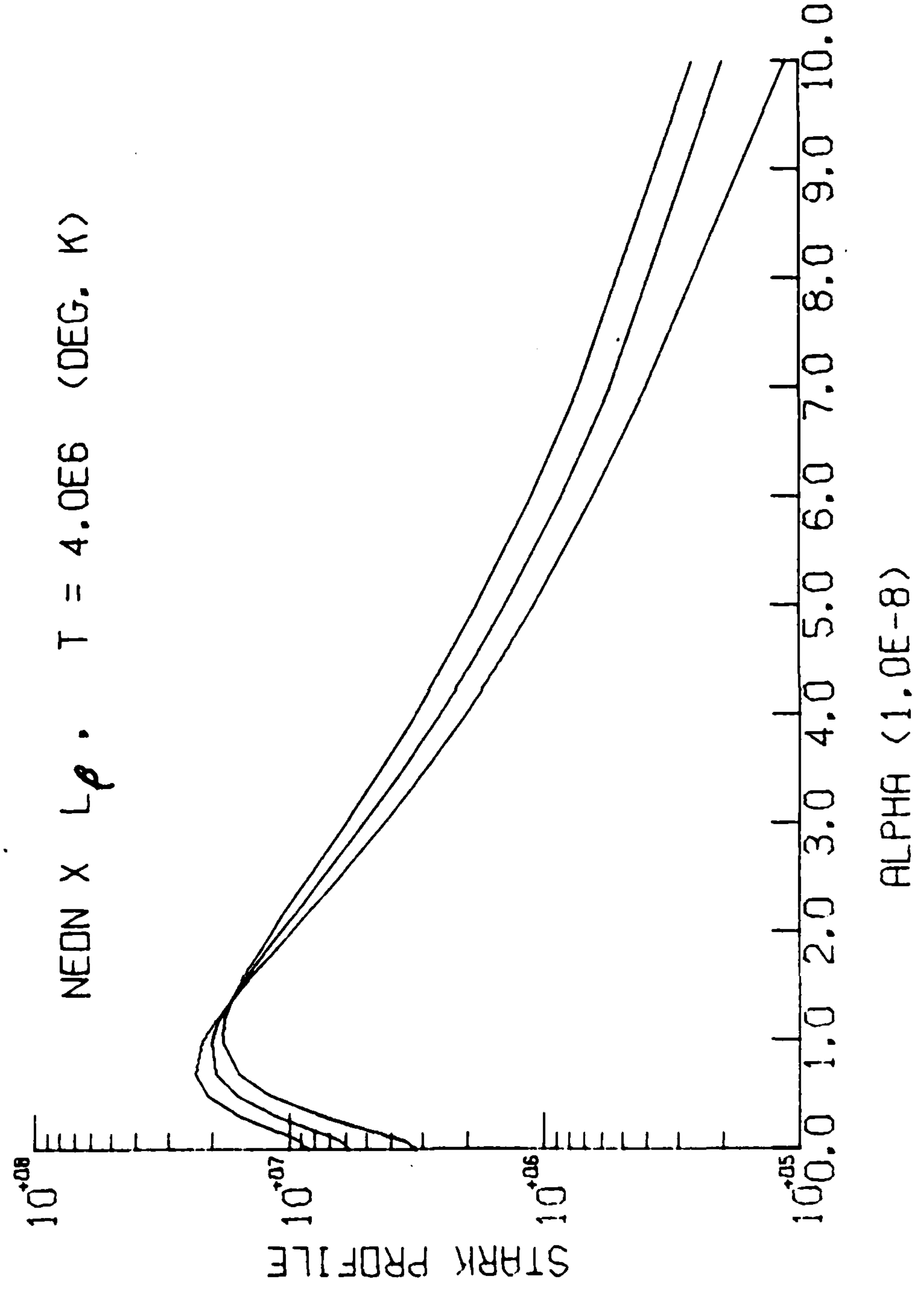

NEON X Lβ . T = 4.0E6 (DEG. K)
STARK PROFILE
10+08
10+07
10+06
10+05
ALPHA (1.0E-8)
0.0
1.0
2.0
3.0
4.0
5.0
6.0
7.0
8.0
9.0
10.0

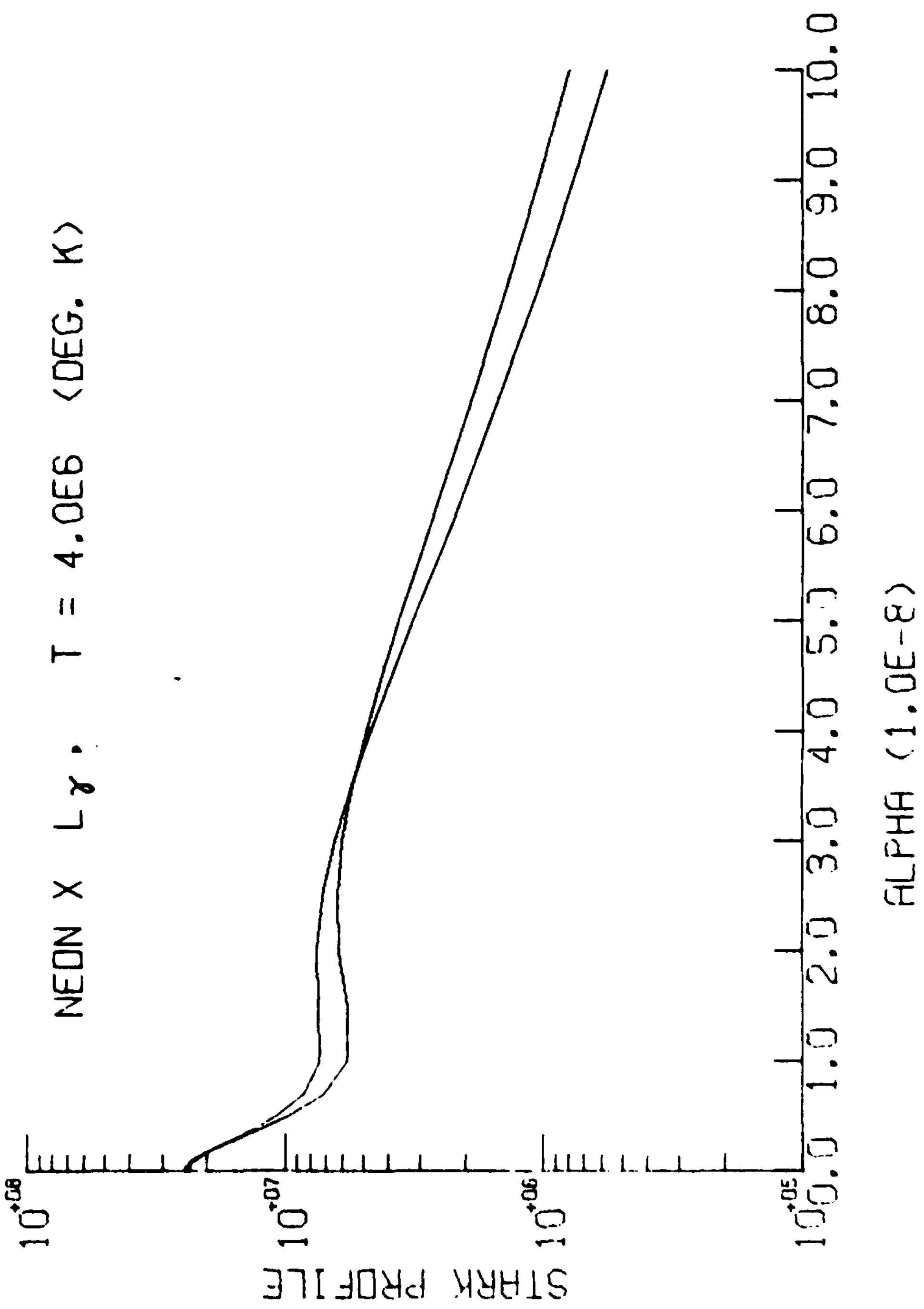
NEON X Lγ, T = 4.0E6 (DEG. K)
STARK PROFILE
ALPHA (1.0E-8)
10+08
10+07
10+06
10+05
0.0
1.0
2.0
3.0
4.0
5.0
6.0
7.0
8.0
9.0
10.0

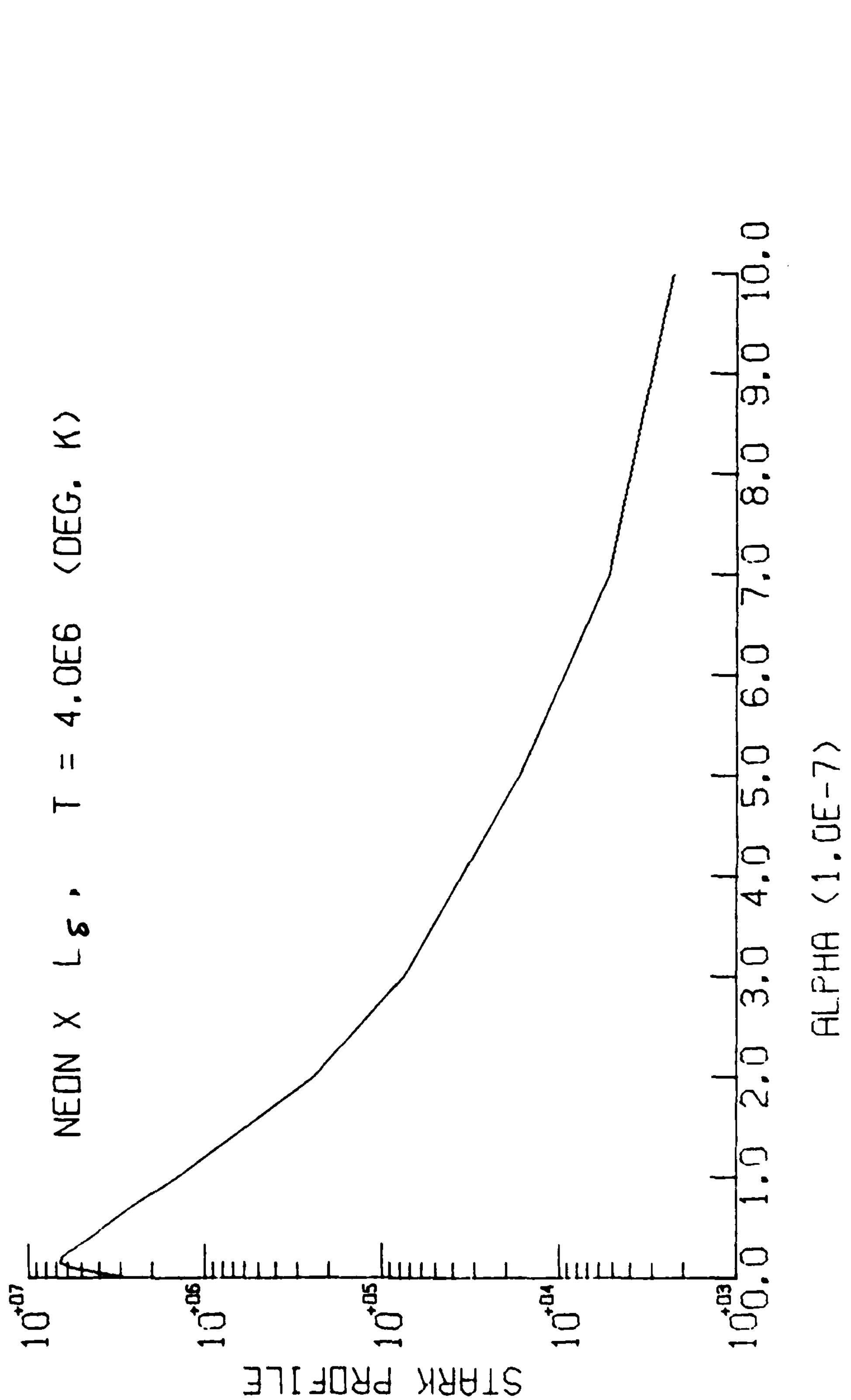

NEON X Lδ, T = 4.0E6 (DEG. K)
STARK PROFILE
ALPHA (1.0E-7)
10^{+07}
10^{+06}
10^{+05}
10^{+04}
10^{+03}
0.0
1.0
2.0
3.0
4.0
5.0
6.0
7.0
8.0
9.0
10.0

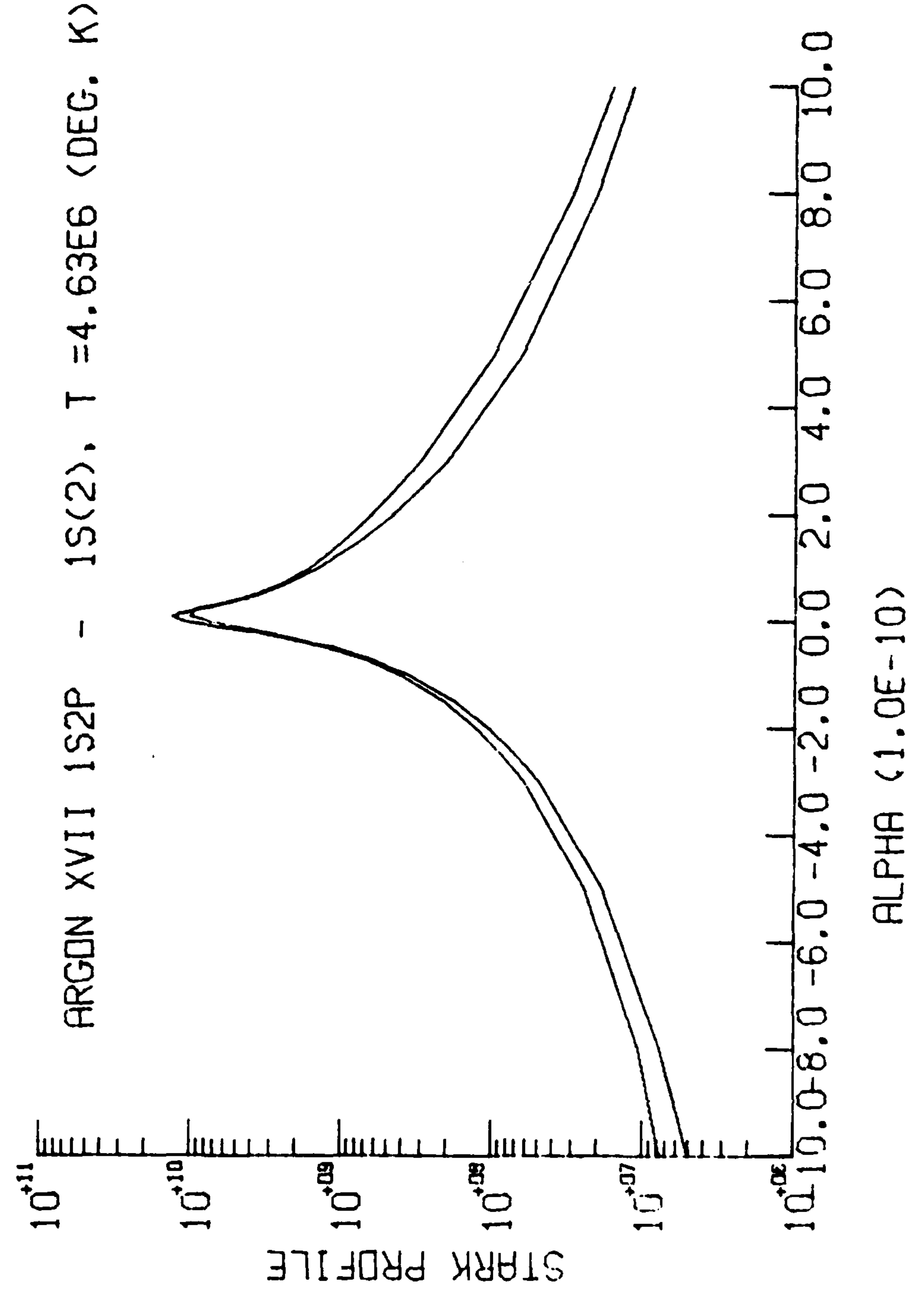
ARGON XVII 1S2P - 1S(2), T =4.63E6 (DEG. K)
STARK PROFILE
ALPHA (1.0E-10)
-10.0 -8.0 -6.0 -4.0 -2.0 0.0 2.0 4.0 6.0 8.0 10.0
10+11
10+10
10+09
10+08
10+07

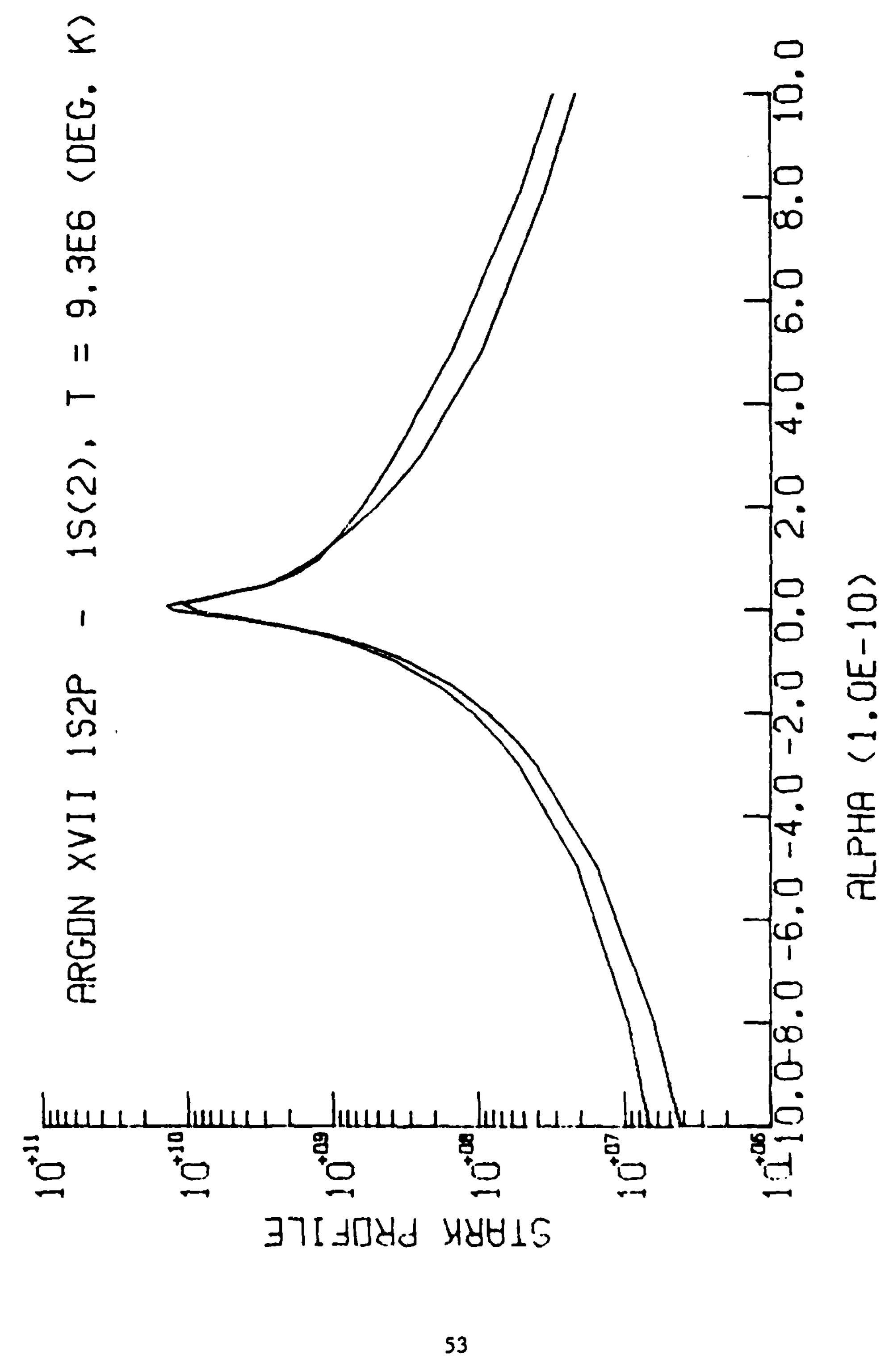
ARGON XVII 1S2P - 1S(2), T = 9.3E6 (DEG. K)
STARK PROFILE
ALPHA (1.0E-10)
-10.0
-8.0
-6.0
-4.0
-2.0
0.0
2.0
4.0
6.0
8.0
10.0
10^{+06}
10^{+07}
10^{+08}
10^{+09}
10^{+10}
10^{+11}

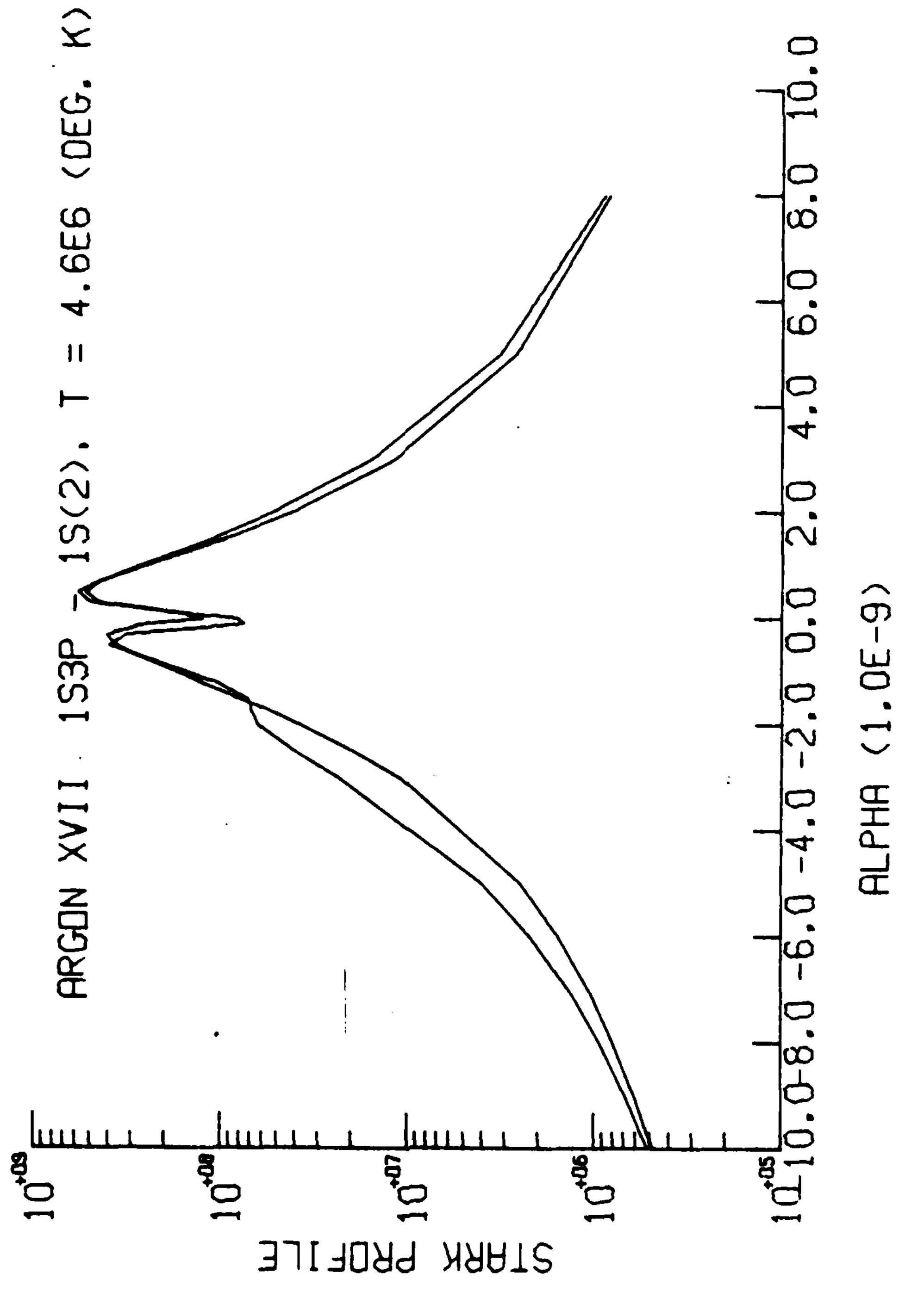
ARGON XVII 1S3P - 1S(2), T = 4.6E6 (DEG. K)
STARK PROFILE
ALPHA (1.0E-9)
10^+05
10^+06
10^+07
10^+08
10^+09
-10.0 -8.0 -6.0 -4.0 -2.0 0.0 2.0 4.0 6.0 8.0 10.0

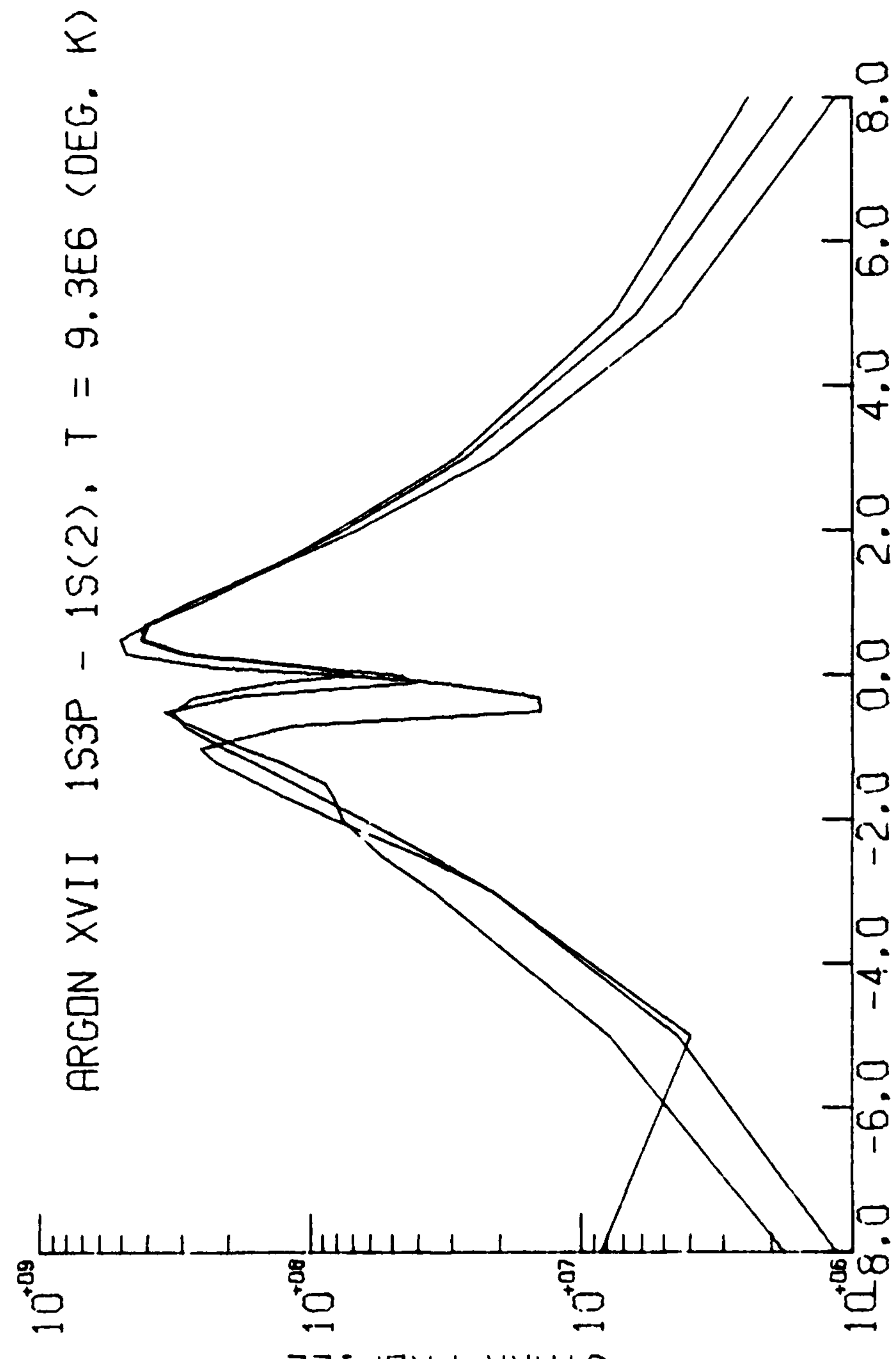
ARGON XVII 1S3P - 1S(2), T = 9.3E6 (DEG. K)
STARK PROFILE
ALPHA (1.0E-9)
-8.0
-6.0
-4.0
-2.0
0.0
2.0
4.0
6.0
8.0

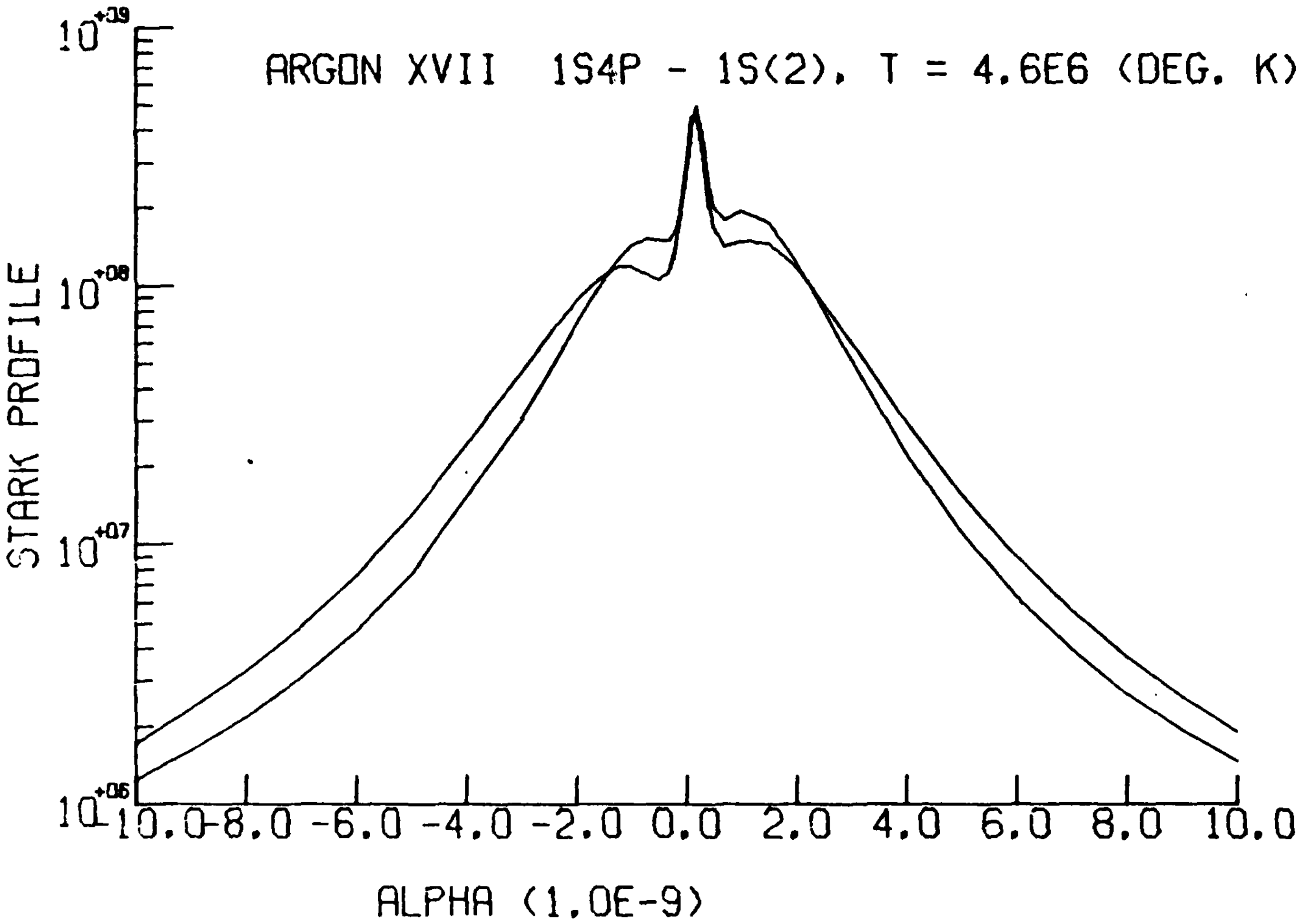
ARGON XVII 1S4P - 1S(2), T = 4.6E6 (DEG. K)
STARK PROFILE
10+09
10+08
10+07
10+06
-10.0 -8.0 -6.0 -4.0 -2.0 0.0 2.0 4.0 6.0 8.0 10.0
ALPHA (1.0E-9)

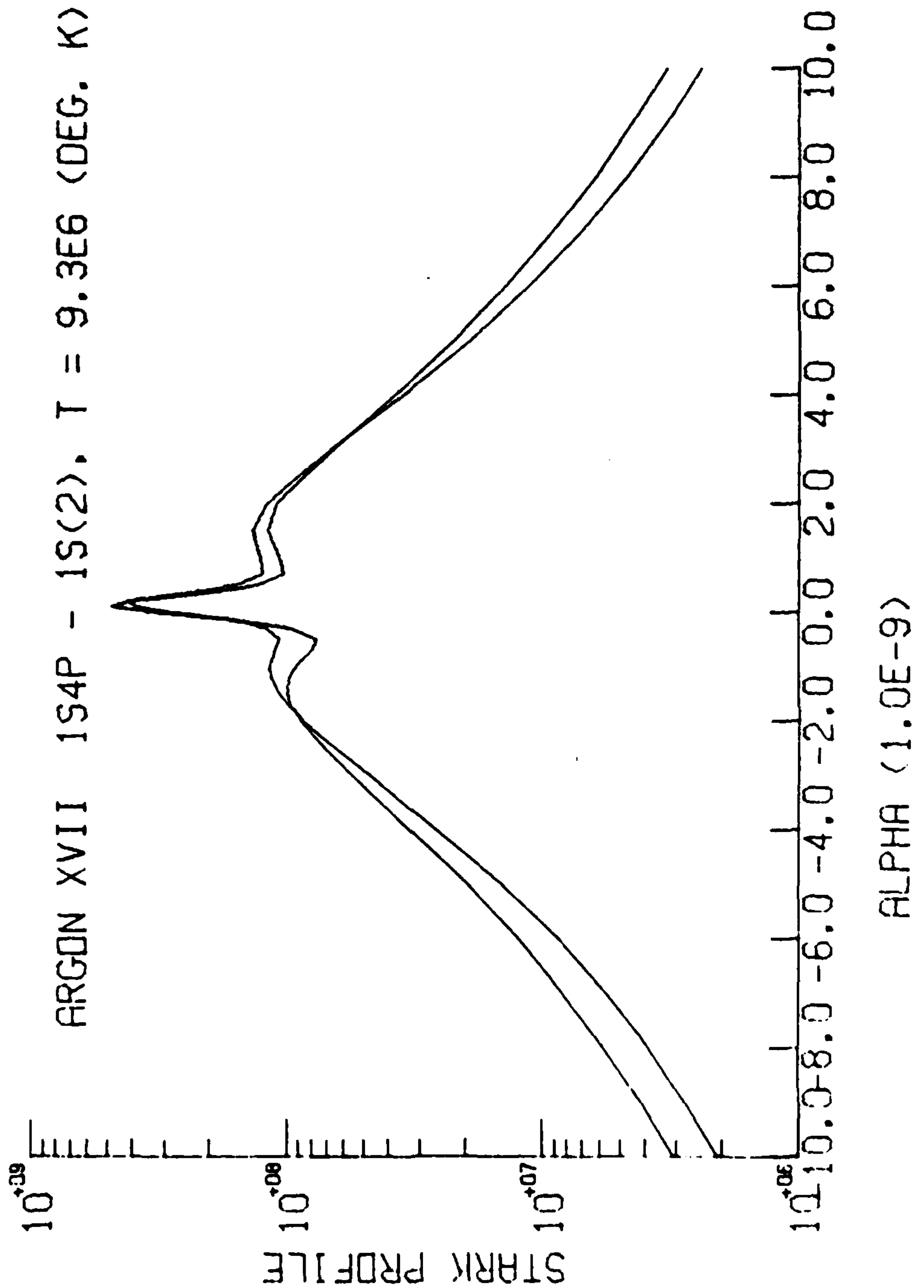
ARGON XVII 1S4P - 1S(2). T = 9.3E6 (DEG. K)
STARK PROFILE
ALPHA (1.0E-9)
-10.0 -8.0 -6.0 -4.0 -2.0 0.0 2.0 4.0 6.0 8.0 10.0

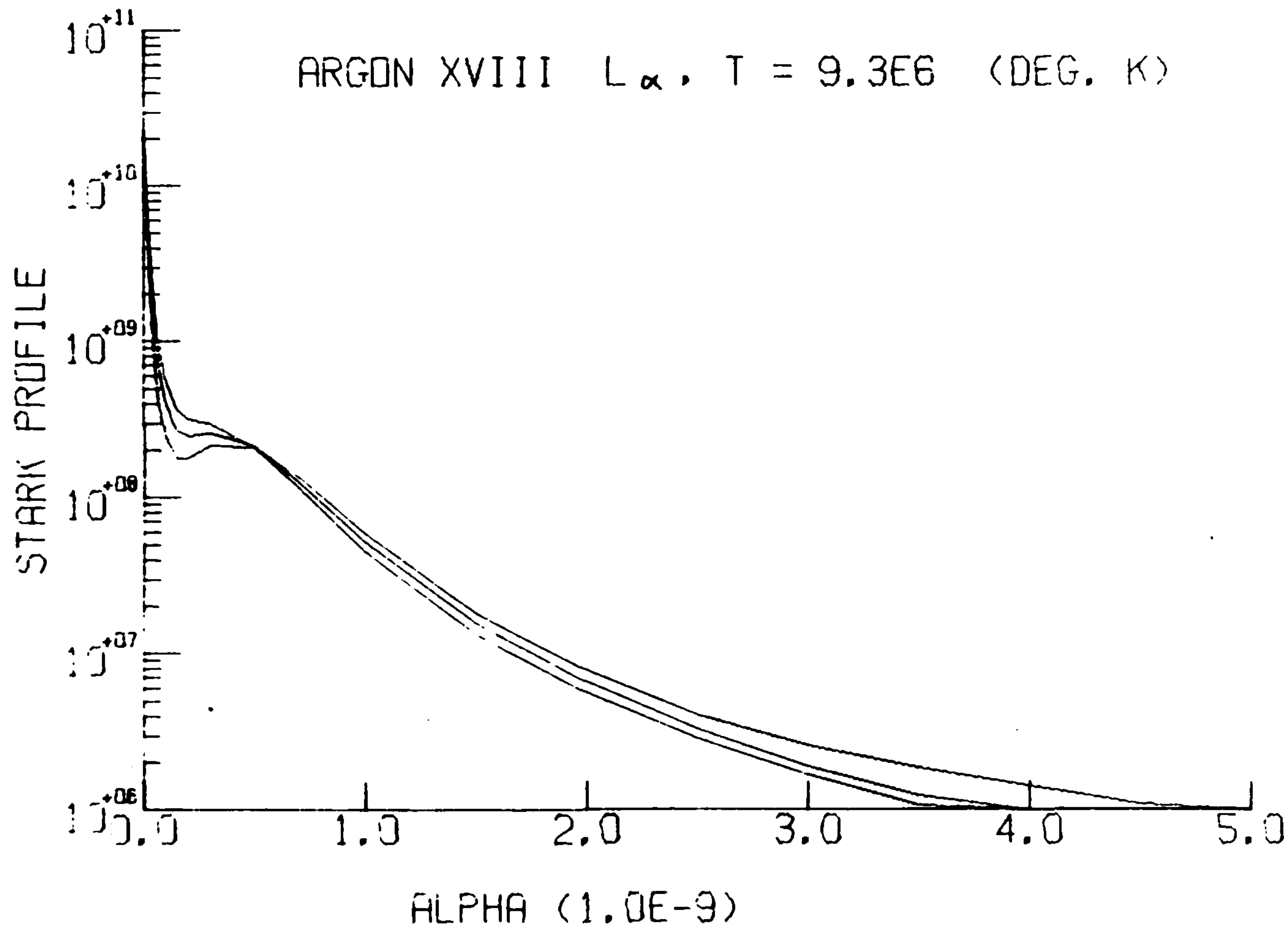
ARGON XVIII Lα, T = 9.3E6 (DEG. K)
STARK PROFILE
10+11
10+10
10+09
10+08
10+07
10+06
0.0
1.0
2.0
3.0
4.0
5.0
ALPHA (1.0E-9)

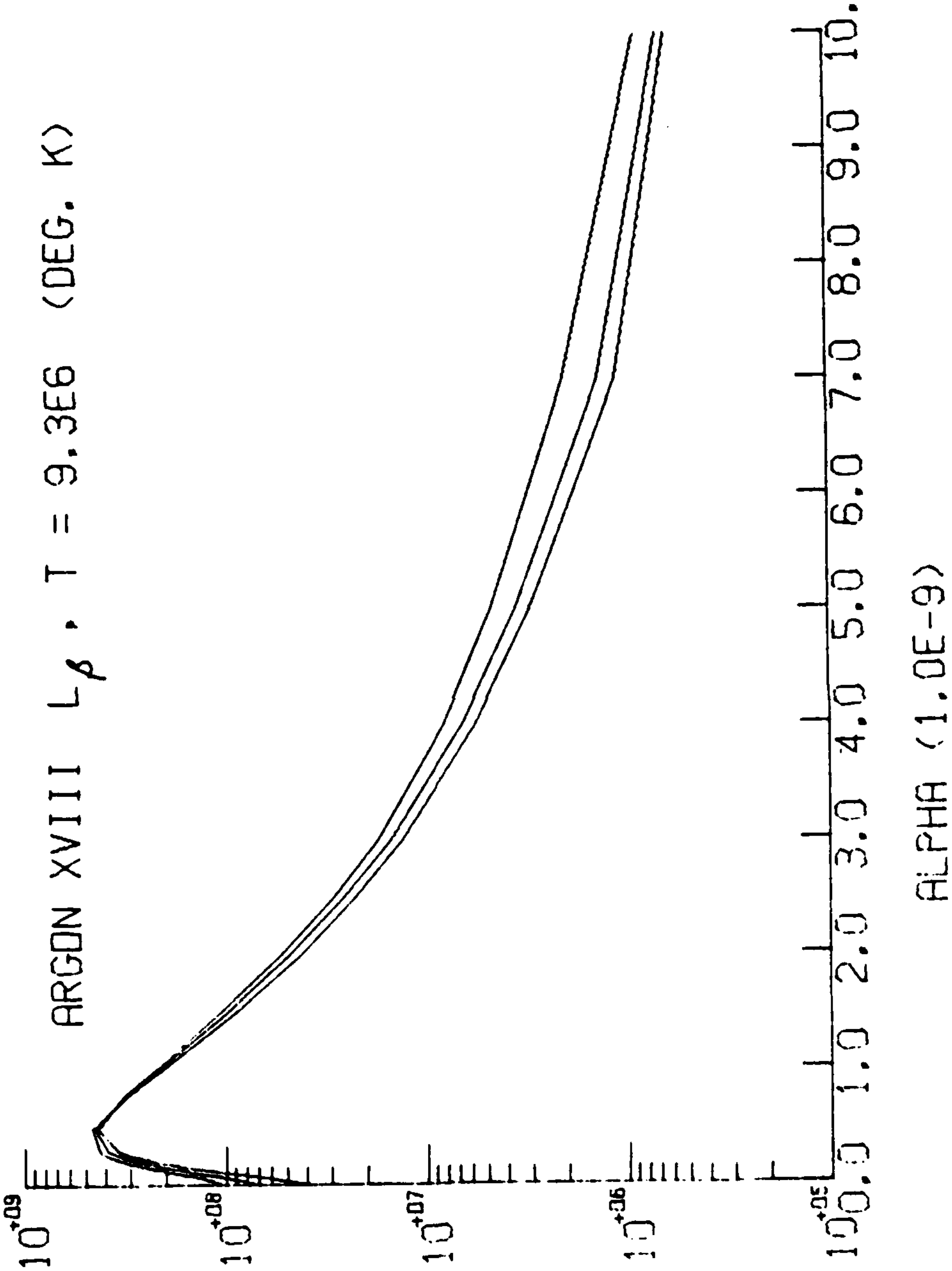

ARGON XVIII L_β , T = 9.3E6 (DEG. K)
STARK PROFILE
ALPHA (1.0E-9)
10^{+09}
10^{+08}
10^{+07}
10^{+06}
10^{+05}
0.0
1.0
2.0
3.0
4.0
5.0
6.0
7.0
8.0
9.0
10.0

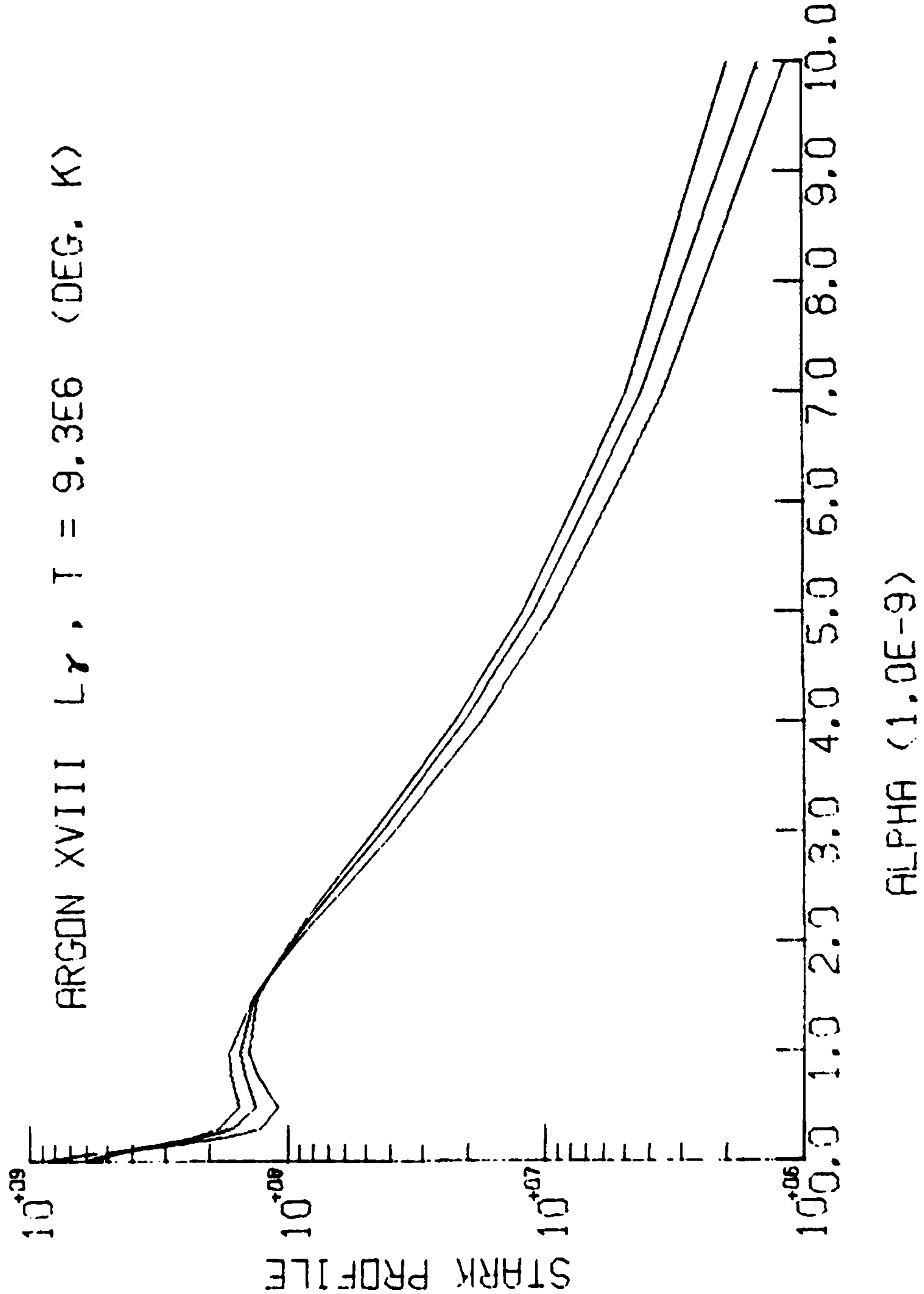
ARGON XVIII Lγ , T = 9.3E6 (DEG. K)
STARK PROFILE
ALPHA (1.0E-9)
0.0
1.0
2.0
3.0
4.0
5.0
6.0
7.0
8.0
9.0
10.0
10+09
10+08
10+07
10+06

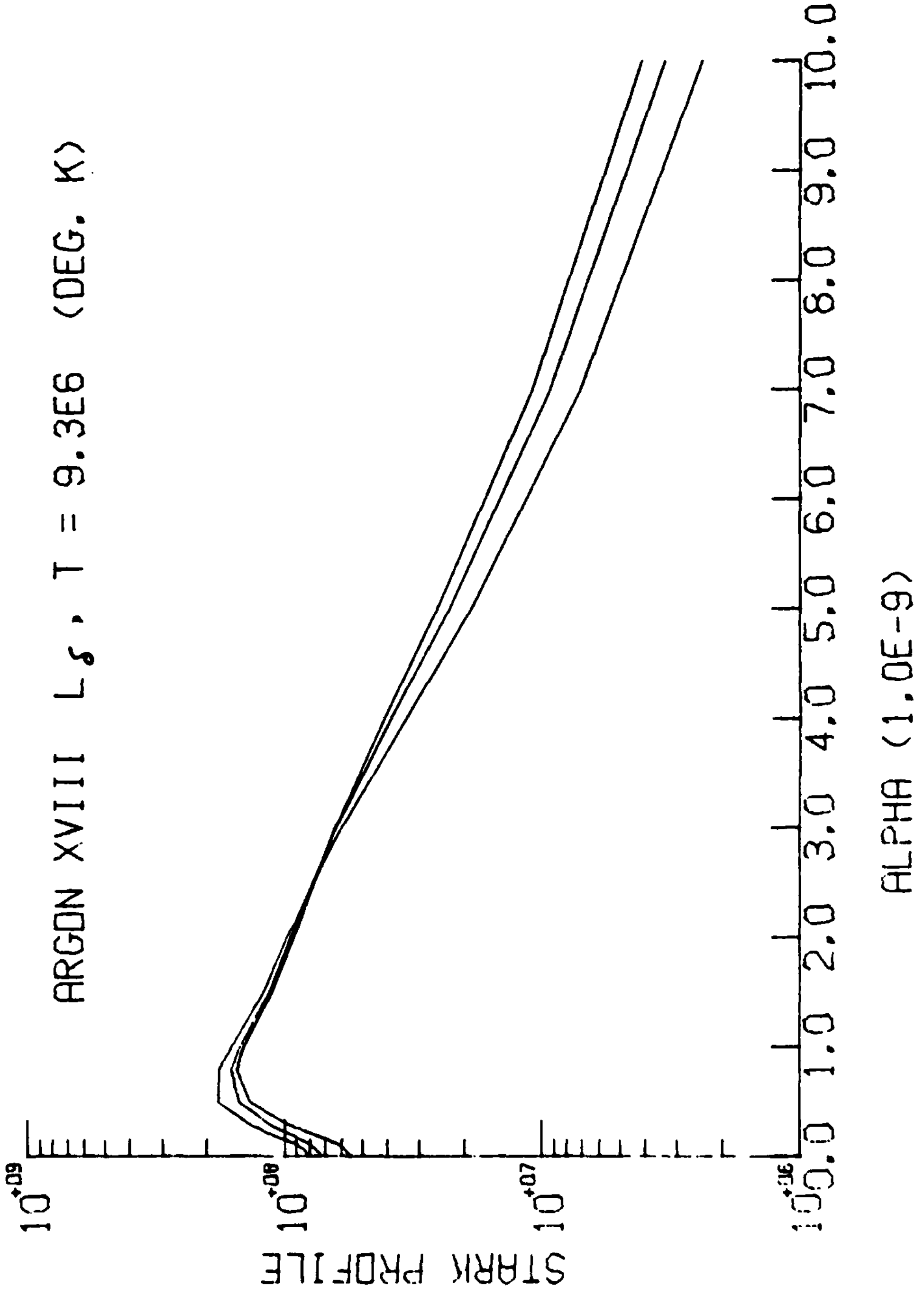

ARGON XVIII Lδ, T = 9.3E6 (DEG. K)
STARK PROFILE
ALPHA (1.0E-9)
10^{+09}
10^{+08}
10^{+07}
10^{+06}
0.0
1.0
2.0
3.0
4.0
5.0
6.0
7.0
8.0
9.0
10.0

ACKNOWLEDGMENTS

The authors wish to thank Dr. Allen Hauer of the Los Alamos Scientific Laboratory for valuable discussions and guidance in this work; they would also like to thank Dr. Jack Davis of the Naval Research Laboratory for direction and assistance in performing the calculations.

This work was supported by the Los Alamos Scientific Laboratory.

DAT
FILM
7-8